



PCCP

**Bell inequalities for entangled qubits: Quantitative tests of quantum character and nonlocality on quantum computers**

Journal:	<i>Physical Chemistry Chemical Physics</i>
Manuscript ID	CP-ART-10-2020-005444.R1
Article Type:	Paper
Date Submitted by the Author:	15-Dec-2020
Complete List of Authors:	Wang, David; Michigan State University, Chemistry Gauthier, Aidan; Michigan State University, Chemistry Siegmund, Ashley; Michigan State University, Chemistry Hunt, Katharine; Michigan State University, Chemistry

SCHOLARONE™  
Manuscripts

**Bell inequalities for entangled qubits: Quantitative tests  
of quantum character and nonlocality on quantum computers**

**David Z. Wang, Aidan Q. Gauthier, Ashley E. Siegmund, and Katharine L. C. Hunt**  
**Department of Chemistry**  
**Michigan State University**  
**East Lansing, MI, USA 48824**

**and**

**Michigan State University St. Andrews Facility**  
**Midland, MI, USA 48640**

**Abstract:** This work provides quantitative tests of the extent of violation of two inequalities applicable to qubits coupled into Bell states, using IBM's publicly accessible quantum computers. Violations of the inequalities are well established. Our purpose is not to test the inequalities, but rather to determine how well quantum mechanical predictions can be reproduced on quantum computers, given their current fault rates. We present results for the spin projections of two entangled qubits, along three axes A, B, and C, with a fixed angle  $\theta$  between A and B and a range of angles  $\theta'$  between B and C. For any classical object that can be characterized by three observables with two possible values, inequalities govern relationships among the probabilities of outcomes for the observables, taken pairwise. From set theory, these inequalities must be satisfied by all such classical objects; but quantum systems may violate the inequalities. We have detected clear-cut violations of one inequality in runs on IBM's publicly accessible quantum computers. The Clauser-Horne-Shimony-Holt (CHSH) inequality governs a linear combination  $S$  of expectation values of products of spin projections, taken pairwise. Finding  $S > 2$  rules out local, hidden variable theories for entangled quantum systems. We obtained values of  $S$  greater than 2 in our runs prior to error mitigation. To reduce the quantitative errors, we used a modification of the error-mitigation procedure in the IBM documentation. We prepared a pair of qubits in the state  $|00\rangle$ , found the probabilities to observe the states  $|00\rangle$ ,  $|01\rangle$ ,  $|10\rangle$ , and  $|11\rangle$  in multiple runs, and used that information to construct the first column of an error matrix  $M$ . We repeated this procedure for states prepared as  $|01\rangle$ ,  $|10\rangle$ , and  $|11\rangle$  to construct the full matrix  $M$ , whose inverse is the filtering matrix. After applying filtering matrices to our averaged outcomes, we have found good quantitative agreement between the quantum computer output and the quantum mechanical predictions for the extent of violation of both inequalities as functions of  $\theta'$ .

## I. Introduction

Bell introduced a set of experimentally testable inequalities with the goal of proving that local hidden-variable theories cannot reproduce observations.<sup>1,2</sup> The inequalities are derived for two-qubit Bell states, which exhibit entanglement. Bell originally worked with singlet-coupled spins,<sup>1</sup> but related inequalities can be derived for the combination of triplet states,

$$|\Psi\rangle = 1/2^{1/2} [ |\alpha(1)\alpha(2)\rangle + |\beta(1)\beta(2)\rangle ], \quad (1)$$

where  $\alpha(k)$  denotes the state of qubit  $k$  with spin projection  $\hbar/2$  along the  $\mathbf{z}$  axis, and  $\beta(k)$  denotes the state of qubit  $k$  with projection  $-\hbar/2$  along  $\mathbf{z}$ .

The current work provides quantitative results for two Bell-type inequalities that apply to qubits coupled into Bell states. The purpose of this work is to determine how well the output from current quantum computers can match quantum mechanical calculations given the current fault rates, rather than to test for the violation of the Bell inequalities *per se*, since violation of the inequalities is well established. The results also provide a useful benchmark for the current accuracy of IBM's publicly accessible quantum computers.

Our results have been obtained from runs on quantum computers through the IBM Q Experience<sup>®</sup>.<sup>3</sup> The first inequality, in a form that was suggested by Polkinghorne,<sup>4</sup> governs the probabilities of finding spins aligned or opposed along three distinct axes A, B, and C. The second inequality, devised by Clauser, Horne, Shimony, and Holt (CHSH),<sup>5</sup> governs a linear combination of correlations between spin projections on different axes. We have observed violations of both inequalities, establishing the non-classical character of the coupled qubits and the impossibility of constructing a local hidden-variable theory that accounts for the measured outcomes. Violation of these inequalities is related to the quantum behavior described as “spooky action at a distance” by Einstein, Podolsky, and Rosen.<sup>6</sup>

Quantum computing offers the potential to solve important, but very difficult problems that cannot be handled by classical computers, due to the exponential scaling of the computational time required. In contrast to classical qubits, which take a definite value (either 0 or 1) at any instant in time, a quantum bit (qubit) may exist in a complex superposition of states  $|0\rangle$  and  $|1\rangle$ . As a result, a very large number of calculations can be run simultaneously on quantum computers, with the state of each qubit “collapsed” to  $|0\rangle$  or  $|1\rangle$  only upon measurement. The prospect for high-speed quantum computation was discussed by Feynman<sup>7</sup> in the early 1980’s. Deutsch and Josza<sup>8,9</sup> subsequently proved that a type of quantum algorithm could run exponentially faster than any conceivable algorithm on a classical computer (see also Cleve *et al.*<sup>10</sup>).

Rapid developments are now occurring with the goal of converting the potential of quantum computing into practice. Recent reviews of the current state of the art in quantum chemistry have been provided by McArdle *et al.*<sup>11</sup> and by Cao *et al.*;<sup>12</sup> early discussions of the complexity of chemical problems in the context of quantum computation have been given by Veis and Pittner,<sup>13</sup> Yung *et al.*,<sup>14</sup> and Kais, Rice, and Dinner;<sup>15</sup> see also Aspuru-Guzik, Lindh, and Reiher.<sup>16</sup> Quantum computational versions exist for both first-quantized and second-quantized methods. In the implementation of first quantization methods on grids, the Born-Oppenheimer approximation need not be invoked.<sup>11,17</sup> Second quantization methods rely on transformations of the Jordan-Wigner occupation-number representation,<sup>18</sup> which include the Bravyi-Kitaev encoding<sup>19-22</sup> with tree-mapping<sup>23</sup> and super-fast versions.<sup>19</sup> Disentangled unitary coupled cluster wave functions have been proven to exactly parametrize any state,<sup>24</sup> thus permitting Trotter-error-free<sup>25</sup> applications in quantum computing. Quantum unitary coupled cluster algorithms with selected subsets of excitations have been applied to many-electron molecules with strong correlation<sup>26</sup> and to excited states.<sup>27</sup>

Quantum computers have been used to determine potential energy curves for  $\text{H}_2$ ,<sup>28-32</sup>  $\text{LiH}$ ,<sup>31,32</sup> linear  $\text{BeH}_2$ ,<sup>31</sup>  $\text{HeH}^+$  (with NV defects in diamond as the qubits),<sup>33</sup> for the dissociation of  $\text{H}_3$  into three hydrogen atoms,<sup>34</sup> for rectangular, linear, and trapezoidal  $\text{H}_4$ ,<sup>27,35</sup> and for linear  $\text{H}_6$  and  $\text{H}_8$ .<sup>36</sup> Calculations for  $\text{H}_2\text{O}$  on a trapped-ion quantum computer have been reported,<sup>37</sup> as well as calculations on  $\text{H}_2\text{O}$  with symmetric stretching.<sup>38,39</sup> Hybrid quantum-classical methods employing neural networks have also been developed.<sup>40</sup>

Smart, Schuster, and Mazziotti<sup>41</sup> have used quantum computing to test the generalized Pauli constraints<sup>42,43</sup> that apply to the eigenvalues of the one-electron reduced density matrix (occupation numbers), and have found no violations. The results suggest limitations on the use of entanglement for quantum control,<sup>44</sup> and restrictions on many-qubit systems in pure states.<sup>45</sup>

The current work focuses on the indications of quantum character of the qubits evidenced in runs on IBM's publicly accessible quantum computers, rather than on quantum supremacy. The results reported here could be simulated, but not directly produced by bits on a classical computer, because they depend on qubit entanglement.

We have found few previously reported tests of the Bell inequalities on quantum computers, and none with the type or extent of exploration in this work. Sisodia<sup>46</sup> has compared the performance of four of IBM's 5-qubit backends when preparing Bell states; he has also determined the density matrices for four 2-qubit states of the Bell type. Huffman and Mizel<sup>47</sup> have proven that measurement changes the state of the qubit  $q[2]$  on an IBM quantum computer, violating a classical inequality suggested by Leggett and Garg.<sup>48</sup> Hamamura<sup>49</sup> has employed the duality between the state space and an "effects space" to show that a dual version of the CHSH inequality<sup>5</sup> is violated on IBM's quantum computers. Pozzobom and Maziero<sup>50</sup> have prepared tunable Bell states on the IBM Yorktown 5-qubit computer and then determined state properties

including fidelity, nonlocal coherence, discord, entanglement negativity, and steering.<sup>50</sup> They found good fidelity, but the remaining properties did not generally fit the quantum predictions, in the absence of a noise model. Alsina and Latorre<sup>51</sup> have used a five-qubit IBM computer to test the Mermin inequalities<sup>52</sup> that apply to three, four, and five entangled particles

Ansmann *et al.*<sup>53</sup> have demonstrated the violation of the CHSH inequality for Josephson phase qubits acting as spin-1/2 particles. They ran single-shot experiments and found  $S = 2.0732 \pm 0.0003$ , thus exceeding the locality threshold ( $S = 2$ ) by 244 standard deviations. Likewise, the qubits in the IBM computers are superconducting transmon qubits,<sup>3,54,55</sup> which employ a nonlinear qubit inductor, such as a Josephson junction operating at a temperature of 15 millikelvin.<sup>3</sup> The anharmonicity of the physical circuit is exploited in order to effectively isolate two basis states, which function as  $|0\rangle$  and  $|1\rangle$ .<sup>3</sup> These are not the spin states of a spin-1/2 particle, but the qubits respond to the quantum gates, such as the Hadamard gate,<sup>56</sup> rotation gates, and coupling between qubits accomplished with controlled-not (C-NOT) gates,<sup>56</sup> in the same way that spin-1/2 particles would respond. With IBM's qiskit<sup>®</sup>,<sup>57</sup> the states of individual qubits and of multi-qubit systems can be visualized on the Bloch sphere.<sup>58</sup> The states and outcomes of measurements on the qubits are described below in terms of spins, for simplicity.

Brunner *et al.* have remarked that Bell's theorem "arguably ranks among the most profound scientific discoveries ever made."<sup>59</sup> Violation of the Bell inequalities was first confirmed experimentally by Freedman and Clauser<sup>60</sup> in 1972, in studies of the polarization of entangled photons created in atomic cascades. In this work, a general CHSH Bell inequality was found to be violated by six standard deviations. Loopholes in the original demonstrations of nonlocality involve potentially inaccurate identification of pairs of particles based on coincidence measurements;<sup>61,62</sup> detector inefficiency,<sup>63-66</sup> which permits a number of systems to elude

observation; and the “memory loophole,”<sup>67</sup> whereby the hidden variables for a pair may include previous measurement choices and outcomes. The loophole connected with pair identification and the detector efficiency loophole do not arise in the current case; and they have been closed in laboratory experiments.<sup>61,62,66,68-70</sup> We have used the definition of locality suggested by Brunner *et al.*,<sup>59</sup> which ensures the independence of pairs of observations, but does not explicitly include the separation between the observers nor the time required for a light signal to pass between them.

Experiments conducted by Fry and Thompson<sup>71</sup> and by Aspect, Grangier, and Roger<sup>72,73</sup> have shown that  $S$  in the CHSH inequality may exceed 2. In the initial experiments by Aspect *et al.*,<sup>72,73</sup> the orientations of the polarizers were fixed in any given set of runs. This left the memory loophole open, by potentially allowing for signals about the polarizer orientations to pass between the two observation sites. Aspect, Dalibard, and Roger<sup>74</sup> closed this the loophole in experiments where the orientations of the two polarizers were changed by acousto-optical switches while the photons in any given pair were in flight. No signal about the orientations could pass between the detectors without exceeding the speed of light.

Tittel, Brendel, Zbinden, and Gisin<sup>75</sup> have reported the violation of the Bell inequalities by entangled photons separated by more than 10 km; Fedrizzi *et al.*<sup>76</sup> subsequently extended this record to 144 km. A quantum random number generator has been used by Weihs *et al.*<sup>77</sup> to select the polarizer orientations. Real-time observations of stars in the Milky Way have also been used to generate random numbers.<sup>78</sup> Experiments have demonstrated entanglement between defect sites in diamond,<sup>79,80</sup> between the electron and nuclear spin of a phosphorus atom embedded in silicon,<sup>81</sup> between opto-mechanical oscillators in silicon,<sup>82</sup>  $\text{Be}^+$  ions,<sup>83</sup>  $\text{Yb}^+$  ions,<sup>84</sup> trapped Rb atoms in excited states,<sup>85</sup> a photon entangled with  $^{138}\text{Ba}^+$ ,<sup>86</sup> and coupled photons.<sup>75-78,87-89</sup>



Greenberger, Horne, and Zeilinger have demonstrated purely quantum behavior without the use of inequalities for three spin-1/2 systems coupled into “Schrödinger’s cat” states,<sup>90</sup>

$$|\Psi\rangle = 1/2^{1/2} ( |\alpha(1)\alpha(2)\alpha(3)\rangle + |\beta(1)\beta(2)\beta(3)\rangle ) . \quad (2)$$

If three observers A, B, and C each make measurements of the spin projection (scaled to  $\pm 1$ ) in either the x or y direction for one of the entangled systems, their results will satisfy the conditions  $A_x B_x C_x = 1$ , but  $A_x B_y C_y = -1$ ,  $A_y B_x C_y = -1$  and  $A_y B_y C_x = -1$ . The product of the last three equalities gives  $-1$ , contradicting the first equality. Pan *et al.*<sup>91</sup> have prepared GHZ states for photons experimentally; Lavoie, Kaltenbaek, and Resch<sup>92</sup> established definite nonlocality in this case. Dür, Vidal, and Cirac<sup>93</sup> have examined the related W state, which exhibits nonlocality and retains the entanglement of two systems, if the third is lost:

$$|\Psi_W\rangle = 1/3^{1/2} ( |\alpha(1)\alpha(2)\beta(3)\rangle + |\alpha(1)\beta(2)\alpha(3)\rangle + |\beta(1)\alpha(2)\alpha(3)\rangle ) , \quad (3)$$

The W state has been prepared experimentally by Eibl *et al.*<sup>94</sup>

We note that entropic versions of the Bell inequalities<sup>95-110</sup> also show violations, with the maxima occurring for different orientations of the measurement axes than for the standard Bell inequalities. Inequalities in systems with continuous variables<sup>111</sup> and nonlocality involving more than three entangled photons have also been investigated.<sup>112-114</sup>

In Section II, we present the two inequalities that are investigated in this work. In Section III, we describe the construction of the Bell states on the quantum computers, the effects of rotation of the spins, and the construction of the error-mitigation matrices. In Section IV, we present our quantitative results from investigations of the first inequality, which governs probabilities of correlation between the spin projections on different axes. In Section V, we characterize locality with reference to the work Brunner *et al.*,<sup>59</sup> and present our results for violations of the CHSH inequality.<sup>5</sup> Section VI contains a brief summary and conclusions.

## II. Classical inequalities and quantum violations

The two types of inequalities investigated in this work hold for classical objects that can be characterized by three properties, each having two possible measurement outcomes. Inequalities of the first type govern the probabilities of observing specific pairs of values of these properties. The inequalities follow from set theoretic considerations for classical objects; but quantum systems may violate them.

We have tested one of these inequalities, in a form suggested by Polkinghorne;<sup>4</sup> this inequality applies to measurements of the spin projections of entangled spin-1/2 particles along axes A, B, and C. The spin measurements yield the probability  $p(A^+B^+)$  to observe spin up (+) for one particle along axis A and spin up for the other along axis B; similarly, the measurements yield the probability  $p(A^+C^+)$  for spin up along both axes A and C, and the probability  $p(B^+C^-)$  for spin up along axis B, but down (-) along axis C. Constraints on the probabilities such as

$$p(A^+B^+) \leq p(A^+C^+) + p(B^+C^-) \quad (4)$$

follow from set theoretic constraints if each of the particles can be placed into one of the eight mutually exclusive categories  $A^+B^+C^+$ ,  $A^+B^+C^-$ ,  $A^+B^-C^+$ ,  $A^+B^-C^-$ ,  $A^-B^+C^+$ ,  $A^-B^+C^-$ ,  $A^-B^-C^+$ , and  $A^-B^-C^-$ .<sup>4</sup> For classical objects of this type, the number  $N(A^+B^+)$  that have characteristics  $A^+$  and  $B^+$  is the sum of the numbers with  $A^+B^+C^+$  and with  $A^+B^+C^-$ ,<sup>4</sup>

$$N(A^+B^+) = N(A^+B^+C^+) + N(A^+B^+C^-) . \quad (5)$$

Also

$$N(A^+C^+) = N(A^+B^+C^+) + N(A^+B^-C^+) , \text{ and} \quad (6)$$

$$N(B^+C^-) = N(A^+B^+C^-) + N(A^-B^+C^-) . \quad (7)$$

Since the numbers in each category must be greater than or equal to zero, an inequality is produced by adding  $N(A^+B^-C^+)$  and  $N(A^-B^+C^-)$  to the right-hand-side of Eq. (5) and using Eqs. (6) and (7),

$$\begin{aligned} N(A^+B^+) &\leq N(A^+B^+C^+) + N(A^+B^-C^+) + N(A^+B^+C^-) + N(A^-B^+C^-) \\ &\leq N(A^+C^+) + N(B^+C^-) . \end{aligned} \quad (8)$$

Analogous reasoning yields

$$N(A^-B^-) \leq N(A^-C^-) + N(B^-C^+) . \quad (9)$$

In terms of the probabilities  $p(A^+B^+)$  and  $p(A^-B^-)$ , we find

$$p(A^+B^+) + p(A^-B^-) \leq [p(A^+C^+) + p(A^-C^-)] + [p(B^+C^-) + p(B^-C^+)] . \quad (10)$$

The classification into eight mutually exclusive categories is not possible for a particle of spin-1/2. A particle that is observed to have the spin projection  $\hbar/2$  along the  $\mathbf{z}$  direction has truly *indeterminate* values along other directions, characterized only by probability amplitudes and probabilities. Consequently, the inequality in Eq. (10) is violated for certain orientations of the axes A, B, and C. The analysis for spin-1/2 particles also applies to coupled qubits. A violation of this inequality indicates the essentially quantum character of the entangled qubits.

Of course, the inequality in Eq. (10) cannot be tested directly, because the spin projections of a single qubit cannot be measured along two different axes simultaneously;<sup>1,2,4</sup> but if the qubits are entangled into the linear combination of triplet states  $|\alpha(1)\alpha(2)\rangle$  and  $|\beta(1)\beta(2)\rangle$  as in Eq. (1), the spin projection of qubit 1 can be measured along axis A, while the spin projection for qubit 2 is measured along axis B. Then the outcome for one qubit can be imputed from the outcome for the other.

Inequalities of the second type govern the expectation values of products of outcomes found by two observers, each of whom has a choice of two measurement axes.<sup>1,2,5</sup> We have considered cases where the first observer measures the spin projection  $\sigma_A$  or  $\sigma_B$  of one qubit along axis A or B, and the second observer measures the spin projection  $\sigma_B$  or  $\sigma_C$  of the second, entangled qubit along axis B or C. We use  $\langle \sigma_J \sigma_K \rangle$  to denote the expectation value of the product of the spin

projection measured along the J axis by the first observer and along the K axis by the second observer, with the spin projections scaled to  $\pm 1$  by division by  $\hbar/2$ . In this case, the Bell inequality proposed by Clauser, Horne, Shimony, and Holt (CHSH)<sup>5</sup> takes the form

$$S = \langle \sigma_A \sigma_B \rangle + \langle \sigma_A \sigma_C \rangle + \langle \sigma_B \sigma_B \rangle - \langle \sigma_B \sigma_C \rangle \leq 2, \quad (11)$$

which is applicable for any local, realistic theory. Quantum mechanically, S may exceed 2. A large violation ( $S = 2^{3/2}$ ) is found when the observers make measurements along four distinct axes A, B, C, and D, with A and B perpendicular to each other, C and D perpendicular to each other, and the C, D axis system rotated by  $\pi/4$  relative to the A, B system.<sup>5</sup> In our experiments with three measurement axes A, B, and C, the maximum observable violation of the CHSH inequality is somewhat smaller, at  $S = 5/2$ . However, any violation of the CHSH inequality by a quantum system indicates the presence of nonlocality.<sup>59</sup>

In this work, we compare the observed differences between the left-hand and right-hand sides of the inequalities (10) and (11) with the quantum mechanical predictions. At present, the fault rate of the accessible quantum computers prevents accurate construction of the Bell states in Eq. (1). We have invariably found contributions to the wave function from the states  $|\alpha(1)\beta(2)\rangle$  and  $|\beta(1)\alpha(2)\rangle$ . These contributions have not been eliminated by a type of repetition code (see Sec. III) that checks for the identity of outcomes of spin measurements for the two qubits.<sup>115-117</sup>

Substantially better methods of error mitigation exist,<sup>118-130</sup> but they require more than 5 qubits all together, for Bell-state runs. Shor's original error-correction algorithm used 9 qubits to encode for one logical qubit and correct its errors;<sup>118</sup> Steane's algorithm reduced the requirement to 7 qubits.<sup>119</sup> The methods of Laflamme *et al.*<sup>120</sup> and Bennett *et al.*<sup>121</sup> require 5 qubits (total, the theoretical minimum) to provide error correction for one qubit. The surface code suggested by Kitaev<sup>126</sup> employs two-dimensional qubit grids with nearest-neighbor connectivity.

The difficulty of error correction in Bell-state runs on 5-qubit architecture raises questions about the observability of violations of the inequalities on publicly available quantum computers at present, and about the accuracy of the results. These are the central issues addressed in the current work. In later sections, we show that despite the current fault rates, we have observed clear-cut violations of both inequalities (10) and (11) in the results from several quantum computers, taken directly. Additionally, we have obtained quite good quantitative agreement between quantum mechanical predictions and the results from the quantum computers for the extent of violation of the inequalities, after the application of filtering matrices for error mitigation, as described in Sec. III.

### III. Construction of Bell states, the first inequality, and rotation of spins

We have examined several different methods for the construction of the Bell state in Eq. (1), which can be expressed equivalently as  $|\Psi\rangle = 1/2^{1/2}(|00\rangle + |11\rangle)$ . The first is the simplest. In this case, the Bell state is produced by applying a Hadamard gate (listed below as h) to qubit 0, and then coupling qubit 0 and qubit 1 with a controlled-not gate conditioned on qubit 0 (C-NOT, listed below as cx, applied to q[0] and q[1]) as represented by the input,

```
h q[0];
cx q[0], q[1];
```

Alternative A includes a gate with the Pauli spin matrix  $\sigma_y$  (y), a phase gate (s) represented by the matrix  $\{\{1, 0\}, \{0, i\}\}$ , and a rotation by  $\pi$  around the y axis, ry(pi), in addition to the Hadamard and controlled-not gates,

```
h q[0];
y q[1];
s q[1];
ry(pi) q[1];
cx q[0], q[1];
```

Alternative B is slightly simpler, relying on gates with the Pauli spin matrix  $\sigma_x$  (x) applied to both qubits,

```
h q[0];
x q[1];
cx q[0], q[1];
x q[0];
```

Alternative C differs from B by employing two additional Hadamard gates,

```
h q[0];
x q[1];
cx q[0], q[1];
x q[0];
h q[0];
h q[0];
```

The four methods have different transpiled versions, despite the fact that the square of the Hadamard gate is the identity operator.

Figure 1 shows the averaged results of ten runs with 8192 shots each on five of the IBM quantum computing systems, burlington,<sup>131</sup> vigo,<sup>132</sup> essex,<sup>133</sup> london,<sup>134</sup> and ourense.<sup>135</sup> States with the qubit spins opposed ( $|01\rangle$  and  $|10\rangle$ ) should not be present, but they appear in the output. Their contributions to the output show relatively little variation with the method of constructing the Bell states. For the different methods, the sums of the percentages of the outcomes  $|01\rangle$  and  $|10\rangle$  ranged from 8.430 to 9.064, when averaged over the five systems. At the time of these runs, we found greater variability from system to system than from method to method. The sums of the percentages of the outcomes  $|01\rangle$  and  $|10\rangle$ , averaged over the four methods of constructing the Bell states, ranged from 3.387 on vigo<sup>132</sup> (and 4.337 on ourense<sup>135</sup>) to a high of 18.995 on burlington.<sup>131</sup>

The contributions to the Bell states from  $|00\rangle$  and  $|11\rangle$  should be equal. The observed asymmetry shows somewhat greater variation from method to method than the contributions from the spin-opposed states show. Averaged over the five systems, the sums of the absolute values of the differences between the percentages of the outcome  $|00\rangle$  and the outcome  $|11\rangle$  ranged from below 7.000 for alternatives A and B, to above 10.000 for the simple Bell state construction and alternative C. The asymmetry between  $|00\rangle$  and  $|11\rangle$ , averaged over the four methods of constructing the Bell states, ranged from 5.208 on essex<sup>133</sup> (and 5.789 on ourense<sup>135</sup>) to 11.055 on burlington.<sup>131</sup> These values are all variable, depending on the proximity in time to the daily tuning of the systems and periodic maintenance, but they are reasonably representative.

We examined whether the results might be improved by use of a repetition code,<sup>115-117</sup> to check whether the entangled qubits have identical values. This can be done without a measurement that collapses the wave functions: A third qubit is coupled by a C-NOT gate to qubit 0, and then also coupled by a C-NOT gate to qubit 1. A measurement on the third qubit should yield 0 if

qubits 0 and 1 have identical values—as they should in the Bell states—but it should yield 1 otherwise. We planned to drop the outcomes where this third qubit was in state 1, and renormalize the remaining outcomes to 100%. We used the simplest method of Bell-state construction in this investigation for 20 runs on each of the five systems mentioned above. Prior to any renormalization, the averaged sums of the percentages of the outcomes  $|01\rangle$  and  $|10\rangle$  ranged from 5.164 on vigo<sup>132</sup> to 11.171 on essex,<sup>133</sup> higher in both cases than *without* the repetition code. Renormalization increased these errors. The repetition code did produce an improvement in the results on burlington.<sup>131</sup> It reduced the error by more than a factor of two: the average sum of the percentages of outcomes  $|01\rangle$  and  $|10\rangle$  dropped to 7.697—though this was still higher than the percentages of spin-opposed states on vigo<sup>132</sup> and ourense<sup>135</sup> without any correction.

So at the outset, it was not clear how well the actual extent of violation of the probabilistic inequalities could be matched by measurements on IBM's publicly accessible quantum computers. The accurate representation of the Bell states is one requirement for a quantitative test. The accurate representation of rotations of the qubit spins by various angles is another requirement.

Some of the early discussions of the inequalities apply to singlet-coupled spins. For convenience, we have adapted the inequalities (10) and (11) to apply to the specific linear combination of triplet states  $|\Psi\rangle = 1/2^{1/2} [ |\alpha(1)\alpha(2)\rangle + |\beta(1)\beta(2)\rangle ]$ , which is easily produced on the quantum computers.

An important feature of the combination of triplet states in Eq. (1) is that the spin coupling set up along the  $z$  axis holds along an arbitrary axis. We show this by re-expressing the spin states  $|\alpha\rangle$  and  $|\beta\rangle$  in terms of the eigenstates of a rotated spin matrix. The matrix  $U_R(\theta, \mathbf{n})$  that rotates a qubit spin by an angle  $\theta$  around the axis specified by unit vector  $\mathbf{n} = (n_x, n_y, n_z)$  is<sup>136</sup>

$$U_R(\theta, \mathbf{n}) = \exp(-i \theta \mathbf{n} \cdot \boldsymbol{\sigma}/2) = 1 \cos(\theta/2) - i \mathbf{n} \cdot \boldsymbol{\sigma} \sin(\theta/2) , \quad (12)$$



where  $\boldsymbol{\sigma}$  is the vector of the Pauli spin matrices,  $\sigma_x$ ,  $\sigma_y$ , and  $\sigma_z$ .<sup>136</sup> For example, in terms of  $|\alpha\rangle$  and  $|\beta\rangle$ , the eigenvectors of the spin matrix  $U_R^\dagger(\theta, \mathbf{n}) \sigma_z U_R(\theta, \mathbf{n})$  where  $\mathbf{n} = (0, 1, 0)$  are  $|r\rangle = \cos(\theta/2) |\alpha\rangle - \sin(\theta/2) |\beta\rangle$ , and  $|s\rangle = \sin(\theta/2) |\alpha\rangle + \cos(\theta/2) |\beta\rangle$ . The state  $|r\rangle$  has a spin projection of  $\hbar/2$  along the axis rotated by  $\theta$  in the  $xz$  plane, and  $|s\rangle$  has a spin projection of  $-\hbar/2$ . The transformation between the  $\{|\alpha\rangle, |\beta\rangle\}$  and  $\{|r\rangle, |s\rangle\}$  bases is accomplished by a matrix containing the scalar products of the states,

$$\begin{pmatrix} \langle \alpha | r \rangle & \langle \alpha | s \rangle \\ \langle \beta | r \rangle & \langle \beta | s \rangle \end{pmatrix} = \begin{pmatrix} \cos(\theta/2) & \sin(\theta/2) \\ -\sin(\theta/2) & \cos(\theta/2) \end{pmatrix} \quad (13)$$

After re-expressing  $|\alpha\rangle$  and  $|\beta\rangle$  in terms of  $|r\rangle$  and  $|s\rangle$ , the Bell state in Eq. (1) becomes

$$\begin{aligned} |\Psi\rangle &= 1/2^{1/2} [ |\alpha(1)\alpha(2)\rangle + |\beta(1)\beta(2)\rangle ] \\ &= 1/2^{1/2} \{ [ \cos(\theta/2) |r(1)\rangle + \sin(\theta/2) |s(1)\rangle ] [ \cos(\theta/2) |r(2)\rangle + \sin(\theta/2) |s(2)\rangle ] \\ &\quad + [ \cos(\theta/2) |s(1)\rangle - \sin(\theta/2) |r(1)\rangle ] [ \cos(\theta/2) |s(2)\rangle - \sin(\theta/2) |r(2)\rangle ] \} \\ &= 1/2^{1/2} [ |r(1)r(2)\rangle + |s(1)s(2)\rangle ]. \end{aligned} \quad (14)$$

This feature of coupling along any axis is shared by the singlet-coupled states.

An additional practical issue arises in the measurements on the quantum computers, because the qubit spins can only be measured along the  $\mathbf{z}$  axis. This is easily resolved, because the probability to observe spin up along  $\mathbf{z}$  if the spin is up along an axis  $\mathbf{z}'$  in the  $xz$  plane at angle  $\theta$  is identical to the probability to observe spin up along  $\mathbf{z}'$  if the spin is up along  $\mathbf{z}$ , since  $|\langle \alpha | r \rangle|^2 = |\langle r | \alpha \rangle|^2$ , and similarly for other probabilities that are needed.

In this work, we have considered coplanar axes A, B, and C, with the angle  $\theta$  between axes A and B and the angle  $\theta'$  between axes B and C. Quantum mechanically from Eq. (10), violations of the Bell inequalities for the entangled states (1) occur when

$$\cos^2(\theta/2) \geq \cos^2[(\theta + \theta')/2] + \sin^2(\theta'/2) . \quad (15)$$

The corresponding quantities from the quantum computer outputs are  $p(A^+B^+) + p(A^-B^-)$  on the left and  $[p(A^+C^+) + p(A^-C^-)] + [p(B^+C^-) + p(B^-C^+)]$  on the right. We have evaluated these probabilities quantum mechanically by finding the spin projections for coupled qubits along the axes (A, B), (A, C), and (B, C), taken pairwise. Figure 2a shows the quantum value of  $f(\theta, \theta') \equiv \cos^2(\theta/2) - \cos^2[(\theta + \theta')/2] - \sin^2[\theta'/2]$ , as  $\theta$  and  $\theta'$  range from 0 to  $2\pi$ . Figure 2b shows the regions where  $f(\theta, \theta') > 0$ , and the Bell inequalities are violated, with a cut-off in the horizontal plane for all of the pairs of angles where  $f(\theta, \theta') < 0$ . The maximum value of the function  $f(\theta, \theta')$  is  $1/4$ , which is found when  $\theta = \theta' = \pi/3$ , or  $\theta = \theta' = 5\pi/3$ . The minimum value  $f(\theta, \theta') = -2$  occurs when  $\theta = \theta' = \pi$ , so that axis B runs in the opposite direction to axes A and C. For many angle pairs,  $f(\theta, \theta') = 0$ . Specifically,  $f(\theta, \theta') = 0$  for all values of  $\theta'$  when  $\theta = 0$  or  $\theta = 2\pi$ , and correspondingly  $f(\theta, \theta') = 0$  for all values of  $\theta$  when  $\theta' = 0$  or  $\theta' = 2\pi$ . Also, if  $0 < \theta < \pi$ ,  $f(\theta, \theta') = 0$  when  $\theta' = \pi - \theta$ ; and if  $\pi < \theta < 2\pi$ ,  $f(\theta, \theta') = 0$  when  $\theta' = 3\pi - \theta$ .

As noted, a second major requirement for a quantitative test of the inequalities (1) and (2) is the ability to obtain  $p(A^+B^+) + p(A^-B^-)$  accurately for the Bell states, when axis B is rotated by an angle  $\theta$  with respect to axis A. The result should be  $\cos^2(\theta/2)$ . We evaluated  $p(A^+B^+) + p(A^-B^-)$  for axis B rotated by  $n\pi/30$  relative to axis A, with one run at each  $n$  value, ranging from  $n = 0$  to  $n = 30$ , and 1024, 4096, or 8192 shots. For comparison purposes, we obtained results from runs on the IBM qasm simulator,<sup>137</sup> which exhibits purely statistical error. On the simulator, with a single run of 1024 shots at each angle, the largest absolute value of the deviation from  $\cos^2(\theta/2)$  was 0.024172 at  $19\pi/30$ ; and the mean absolute error was 0.005732. With 4096 shots, the largest absolute value of the deviation from  $\cos^2(\theta/2)$  was 0.02100, at  $\pi/2$ , and the mean absolute error

was 0.004245. With 8192 shots, the largest absolute value of the deviation from  $\cos^2(\theta/2)$  was 0.01368, at  $\pi/2$ , and the mean absolute error was 0.002712.

We looked next at the results from runs at each angle on Burlington.<sup>131</sup> Figure 3 shows the values of  $p(A^+B^+) + p(A^-B^-)$  as a function of  $\theta$ , from sets of ten runs, each with 1024 shots (in red), 4096 shots (in cyan) and 8192 shots (in blue). The results generally agree well with  $\cos^2(\theta/2)$  at  $\theta = \pi/2$ , but they diverge from the expected results for other values of  $\theta$ ; for  $\theta < \pi/2$ , the values of  $p(A^+B^+) + p(A^-B^-)$  are too small, while for  $\theta > \pi/2$ , they are too large. The mean absolute errors are 0.11005 with 1024 shots, 0.09862 with 4096 shots, and 0.10316, with 8192 shots. In a few cases, fluctuations produced clear outliers. This was observed at  $2\pi/3$  and to a greater extent at  $11\pi/15$  and  $14\pi/15$  in the runs with 1024 shots. In these cases, we re-ran the codes three times on burlington<sup>131</sup> with 1024 shots, and averaged the values. The results are plotted in orange, although they are obscured by other points where the values coincide. In the runs with 4096 shots, we found outliers at  $\pi/2$  and  $14\pi/15$ ; results from an average of four new runs at these angles on ourense<sup>135</sup> are plotted in green. Finally, for the runs with 8192 shots, we found outliers at  $\pi/10$  and  $17\pi/30$ ; results from an average of four additional runs on ourense<sup>135</sup> are also plotted, this time in magenta. Overall, the most striking feature of this plot is the regularity of the curve from the quantum computers, especially from the runs with 4096 or 8192 shots—a feature that we did not anticipate. Combined with a lack of significant drop-off in the mean absolute error with an increasing number of shots, this feature suggests that the deviation from  $\cos^2(\theta/2)$  may be systematic.

Accordingly, we constructed an error mitigation matrix that is independent of the previous set of calculations. We have adopted the qiskit procedure<sup>57</sup> for constructing error mitigation matrices on the quantum computers, but we have modified the procedure by applying the matrices to the averaged results, outside of the quantum computing runs. First we allowed the quantum

computer to remain in the two-qubit state  $|00\rangle$ , in 25 calibration runs on Burlington,<sup>131</sup> each with 8192 shots, and then determined the fraction of measurements reported as  $|00\rangle$ ,  $|01\rangle$ ,  $|10\rangle$ , or  $|11\rangle$ . We regard the states  $|01\rangle$ ,  $|10\rangle$ , and  $|11\rangle$ , which should not have appeared in the measurement outcomes, as “intruder” states in this case. The fractions of measurements of each of the possible outcomes go into the first column of the error matrix  $M$ . Next we prepared the two-qubit state  $|01\rangle$ , and again determined the fraction of measurements that were reported as  $|00\rangle$ ,  $|01\rangle$ ,  $|10\rangle$ , or  $|11\rangle$ , to find the second column of the error matrix  $M$ . We repeated this procedure after preparing the states  $|10\rangle$  and  $|11\rangle$  to find the third and fourth columns of  $M$ . In each case, we used sets of 25 calibration runs with 8192 shots. Then we applied the inverse  $M^{-1}$  to the observed outcomes of  $|00\rangle$ ,  $|01\rangle$ ,  $|10\rangle$ , and  $|11\rangle$  for spin projection measurements along various pairs of axes, to obtain the results after error mitigation. The inverse matrices found for Burlington,<sup>131</sup> Vigo,<sup>132</sup> London,<sup>134</sup> and Ourense<sup>135</sup> in the course of this investigation are listed in the Appendix. The stated purpose of the mitigation matrix is to reduce read-out error upon measurement. We note that the qiskit strategy<sup>57</sup> would also ameliorate the effects of incomplete inversion of the qubits and the noise due to stray electromagnetic fields. It is a fair correction for the current application, in the sense that it does not account for errors in rotating the qubits by arbitrary angles, only for  $180^\circ$  inversions (and for leaving the qubit unaltered).

The error-mitigated results are shown in Figure 4, with the same color coding as before: red for the runs with 1024 shots, cyan for runs with 4196 shots, and blue for runs with 8192 shots. The alternate runs for angles where we originally had outliers were mitigated with the same matrix  $M^{-1}$  and color coded as before. The mean absolute errors of the mitigated results are smaller by factors of  $\sim 3$ -6 than the corresponding values for the raw results; for 1024 shots, the mean absolute error is 0.03348, for 4096 shots it is 0.01606, and for 8192 shots it is 0.01868. The fit between the

results with error mitigation and the expected  $\cos^2(\theta/2)$  dependence is greatly improved as shown in Figure 4, relative to the raw results in Figure 3. The error-mitigated results obtained with 4096 and 8192 shots are particularly close to the actual quantum values. Discrepancies are still found to some extent for the A, B angles closest to  $\pi$ ; but overall the quality of the fit suggests that it might be possible to obtain quantitatively accurate results for the violations of the inequalities in Eqs. (10) and (11) on the quantum computers. In the construction of the Bell states, we have observed rather pronounced asymmetries between  $|00\rangle$  and  $|11\rangle$ , along with asymmetries between  $|01\rangle$  and  $|10\rangle$ , which are usually smaller in terms of actual percentages, but may be large on a relative basis. The asymmetries do not affect any of the sums of probabilities  $p(A^+B^+) + p(A^-B^-)$ ,  $p(A^+C^+) + p(A^-C^-)$ , or  $p(B^+C^-) + p(B^-C^+)$  that go into Eq. (10). This feature is favorable, since it increases the likely level of quantitative accuracy.

#### IV. Quantitative tests of the quantum character of coupled qubits

We have computed the differences  $\Delta$  defined as

$$\Delta = p(A^+B^+) + p(A^-B^-) - \{[p(A^+C^+) + p(A^-C^-)] + [p(B^+C^-) + p(B^-C^+)]\} \quad (16)$$

for the Bell states in Eq. (1), for spin projections along one of the coplanar axes A, B, and C for each qubit. We constructed the Bell states for qubits 0 and 1, using the first construction method listed in Sec. II. The angle between axes A and B was fixed at  $\pi/3$  (the location of the maximum value of  $\Delta$ ) in all of the runs, and the angle between axes B and C was varied from 0 to  $\pi$  in steps of  $\pi/24$ . First, we ran ten times with 8192 shots at each of the fixed angles between two axes in order to determine the probabilities of finding the qubit states aligned or opposed. With the ten measured outcomes for each angle pair ( $\theta$  from A to B,  $\theta'$  from B to C, and  $\theta + \theta'$  from A to C), we generated 1000 different combinations of the results, calculated  $\Delta$  for each combination, and then determined the average value of  $\Delta$  for the entire set of 1000 combinations, as well as the standard deviation  $\sigma$ . Quantum mechanically, the expected value of the average is

$$\Delta = \cos^2(\theta/2) - \cos^2[(\theta + \theta')/2] - \sin^2(\theta'/2) . \quad (17)$$

Any case where the value of  $\Delta$  is positive illustrates the purely quantum character of the qubits. If  $\Delta$  is positive, it is impossible to categorize the spin projections along three different axes simultaneously, as one could for a classical object.

From a first set of runs, we determined the average values of  $\Delta$  and the standard deviation  $\sigma$  on IBM's qasm simulator.<sup>137</sup> The results are listed in Table 1. With  $\theta$  fixed at  $\pi/3$ , the average value of  $\Delta$  is positive over the range of  $\theta'$  from  $\pi/24$  to  $5\pi/8$ , as predicted quantum mechanically. For  $\theta'$  equal to 0 or  $2\pi/3$ , the value of  $\Delta$  is small and negative, but it falls within a standard deviation of the quantum expectation value of zero.

The results for  $\Delta$  and  $\sigma$  from the simulator runs are shown in Figure 5. The quantum mechanical prediction is plotted as the blue curve; the red points show the average  $\Delta$  values from the simulator as a function of the angle  $\theta'$ , with error bars extending one standard deviation above and below the average values. It is apparent that the simulator results adhere very closely to the numerical values obtained quantum mechanically, in addition to showing the essentially quantum character of the qubits based on results in the range  $0 < \theta' < 2\pi/3$ . In this case, the standard deviations reflect purely statistical variations.

We have then repeated the sets of 10 runs for each pair of axes, giving 1000 combinations of results in total, using IBM's 5-qubit london quantum computer<sup>134</sup> with 8192 shots for each run. The results are shown in Figure 6 and listed in Table 2. The red points with standard deviations mark the raw results. We have found clear-cut instances where  $\Delta > 0$  in the range of  $\theta'$  values  $\pi/12 \leq \theta' \leq 13\pi/24$ . This is a sub-interval of the range quantum mechanically predicted to show  $\Delta > 0$ , but the results still illustrate the fundamentally quantum nature of the qubits. For the angle  $5\pi/24$ , the raw results are plotted in orange. The initial set of runs gave a value of  $\Delta$  that was slightly out of alignment with the overall pattern of points. The repeat runs gave a value of  $\Delta$  that is closer to the overall pattern, but not very different from the  $\Delta$  value in the first run.

The raw results from runs on IBM's 15-qubit melbourne<sup>138</sup> quantum computer are shown in purple in Figure 6. As before, the values of  $\Delta$  and  $\sigma$  have been obtained from 1000 combinations of 10 runs for each of the angles. The larger number of qubits made it possible to determine the outcomes 00, 01, 10, and 11 for all three angle pairs in each of the runs, with (A, B) on qubits 0 and 1, (A, C) on qubits 2 and 3, and (B, C) on qubits 4 and 5. Each run consisted of 1024 shots. The raw results from melbourne<sup>138</sup> are not as accurate as the raw results from london,<sup>134</sup> and the standard deviations are appreciably higher. The difference is due to the higher fault rate of qubits

on melbourne<sup>138</sup> and the smaller number of shots. In some of the ten individual runs for each set of orientations of the A, B, and, C axes (before combinations of the results were generated), clear-cut violations of the Bell inequalities were observable, however. This holds in seven cases with  $\theta' = \pi/3$ , six cases with  $\theta' = \pi/12$ , seven cases with  $\theta' = \pi/2$ , and three cases with  $\theta' = 7\pi/12$ .

As indicated in Tables 1 and 2, when the calculated A, C angle  $\theta + \theta'$  satisfies  $\pi < \theta + \theta' < 2\pi$ , in the work on the simulator<sup>137</sup> and on london<sup>134</sup> we have replaced the angle by  $2\pi - (\theta + \theta')$ , since the quantum mechanical probabilities  $p(A^+C^+) + p(A^-C^-)$  are identical in both cases, as are the probabilities  $p(A^+C^-) + p(A^-C^+)$ . In the next section, when  $\theta + \theta'$  exceeds  $2\pi$ , we have replaced  $\theta + \theta'$  by  $(\theta + \theta' - 2\pi)$  for the same reason. The average values of the sums of probabilities are compared in Table 3 for the angle pairs  $(\pi/24, 47\pi/24)$ ,  $(\pi/2, 3\pi/2)$ , and  $(23\pi/24, 25\pi/24)$ , for ten runs at each angle on ourense,<sup>135</sup> vigo,<sup>132</sup> and the ibmq qasm simulator.<sup>137</sup> The replacements make very little difference to the results from the simulator. The results from the five-bit quantum computers are not identical for the pairs of angles, but the differences between the results on the two quantum computers are larger than the differences between angles in a pair. The differences in runs separated by nine days are also larger than the differences between angles in a pair. The largest differences between the results for angle pairs are seen in  $p(A^+C^+) - p(A^-C^-)$  and  $p(A^+C^-) - p(A^-C^+)$  on the quantum computers. These differences are quite small on the simulator. In any event, these asymmetries do not affect the results in this section or the next. The angle replacements make the calculations appreciably more efficient, because they let us re-use one set of ten results in eight of the twenty-five cases.

The results for  $\Delta$  after error mitigation by a filtering matrix<sup>57</sup> are plotted as the green points in Figure 6. Given the fault rate noted above, it is interesting that the patterns of both the red points (raw) and the green points (error-mitigated) show a great deal of regularity. The error-mitigated



$\Delta$  values are positive over the entire set of angles studied in the range  $0 < \theta' < 2\pi/3$ , exactly as predicted quantum mechanically. The averaged value of  $\Delta$  found for a B, C angle of 0 should be zero quantum mechanically; the computed value is positive, but it falls within one standard deviation of zero. The error-mitigated value of  $\Delta$  is negative for  $2\pi/3$  and a little less than four standard deviations away from zero.

In the quantum mechanical case, the dividing line between inherently quantum values of  $\Delta$  ( $\Delta > 0$ ) and values that could be consistent with a classical picture is very sharp, as is apparent from analysis of Eq. (17): If  $\theta = \pi/3$ ,  $\Delta = 0$  when  $\theta' = 2\pi/3$ ;  $\Delta > 0$  for  $\theta' < 2\pi/3$  (except for  $\theta' = 0$ ); and  $\Delta < 0$  for  $\theta' > 2\pi/3$ . We have explored the nature of this transition on a quantum computer. For this investigation, we shifted from the london<sup>134</sup> computer to ourense,<sup>135</sup> which generally gave more accurate results. Figure 7 shows the number of cases where the quantum computer gave negative values of  $\Delta$ , out of 1000 tests generated by taking all possible combinations of 10 runs at each of the pairs of angles (A, B), (B, C) and (A, C). For this plot, quantum mechanical calculations would give a Heaviside theta function scaled by 1000, with a jump at  $\theta' = 2\pi/3$ . Results from runs on ourense<sup>135</sup> are plotted for two separate sets of 1000 combinations for the angles  $\theta' = 5\pi/8, 31\pi/48, 11\pi/16, 17\pi/24$ , and then for three separate sets of 1000 combinations for the angles closer to  $2\pi/3$ , specifically  $\theta' = 21\pi/32, 127\pi/192, 2\pi/3, 43\pi/64, \text{ and } 65\pi/96$ . Pronounced fluctuations in the number of combinations within a set that yielded  $\Delta < 0$  are seen at the angles  $\theta' = 2\pi/3, 43\pi/64, \text{ and } 65\pi/96$ , with smaller fluctuations for  $\theta' = 21\pi/32$  and  $127\pi/192$ . On the quantum computer, the transition region is fairly narrow; it runs over a range of  $\sim\pi/96$  in the  $\theta'$  values.

We have found a comparatively high level of agreement between the quantum results for  $\Delta$  and the error-mitigated results obtained with the london<sup>134</sup> computer. We have also obtained an average value of  $\Delta$  that is 9.27 standard deviations above zero on london,<sup>134</sup> when  $\theta' = \pi/3$ . We wanted to see whether it would be possible to come even closer to the maximum value of  $\Delta = 0.25$ , which is predicted to occur when  $\theta' = \pi/3$ . The results of the runs (as above) on london,<sup>134</sup> vigo,<sup>132</sup> and ourense,<sup>135</sup> with and without error mitigation, are plotted in Figure 8. Both vigo<sup>132</sup> and ourense<sup>135</sup> gave values of  $\Delta$  closer to the quantum limit. In fact, the average error-mitigated value on vigo<sup>132</sup> (plotted in blue) slightly exceeded 0.25, although the value is close to falling within a standard deviation of the quantum result. The two sets of runs on ourense<sup>135</sup> were generated over two- to three-day periods, separated by five days. Two different error mitigation matrices, obtained five days apart, were applied to the probability distribution over qubit states on ourense,<sup>135</sup> with quite similar effects. The runs came very close to reproducing the predicted maximum,  $\Delta = 0.25$ . These runs also gave average values of  $\Delta$  that are many standard deviations above zero, even without error mitigation: 22.76 standard deviations above zero on vigo,<sup>132</sup> 20.78 standard deviations above zero in the first set of runs on ourense,<sup>135</sup> and 25.67 standard deviations above zero in the second set of runs on ourense,<sup>135</sup> compared with 28.06 standard deviations above zero on the qasm simulator.<sup>137</sup> This behavior is decidedly non-classical.

## V. Nonlocality and the CHSH inequality

If  $S$  in Eq. (11) exceeds 2, then a number of potential hidden-variable theories are ruled out. The quantity  $S$  is a linear combination of correlations between the spin-projections for two qubits along various axes. In the original form suggested by Clauser, Horne, Shimony, and Holt,<sup>5</sup> four different axes are used, two by the first observer and two by the second observer, with no measurement axes in common. The maximum value of  $S$  obtainable with this version of the CHSH inequality is  $S = 2^{3/2}$ . In our runs with three axes,  $A$ ,  $B$ , and  $C$ , where the first observer measures the spin projection along axis  $A$  or  $B$ , while the second observer measures the spin projection along axis  $B$  or  $C$ , the maximum observable value of  $S$  is slightly smaller at 2.5, but  $S$  is still well over 2.

We have adopted the definition of locality used by Brunner *et al.*,<sup>59</sup> and we have followed their proof of the CHSH inequality,<sup>5</sup> adapted to our 3-axis case. The definition allows for the possibility that values in a set of variables  $\lambda$  (which may be hidden) affect the outcomes of measurements made by the two observers. In a local theory, the probabilities for measurement outcomes  $\sigma_J$  and  $\sigma_K$  should factorize as<sup>59</sup>

$$p(\sigma_J \sigma_K | \lambda) = p_1(\sigma_J | \lambda) p_2(\sigma_K | \lambda) . \quad (18)$$

That is, the probability distribution for the outcomes found by the first observer depends on  $\lambda$  and the local choice of measurement axis  $J$ , but not on the axis chosen nor the outcome found by the second observer. The definition of locality in Eq. (18) refers to the independent factorization of probabilities of the outcomes of measurements by two observers.<sup>59</sup> Strictly, this definition ensures one type of locality: the exclusion of influences by one observer on the other. The distance between the observers is not considered explicitly, nor is the speed of light considered. Limits on the speed of transmission of information between the observers and closure of the “memory

loophole<sup>67</sup> must be incorporated by restrictions on the allowable variables  $\lambda$ . The analysis of locality based on Eq. (18) involves the assumptions that both objects in an entangled pair are accurately identified, and that detection is efficient.<sup>59</sup> Both of these conditions are met in the current work involving coupled qubits.

After we allow for the possibility that  $\lambda$  may vary between runs, as represented by the normalized probability distribution  $q(\lambda)$  of the values of  $\lambda$ , the condition for locality can be cast in the form<sup>59</sup>

$$p(\sigma_J \sigma_K) = \int_{\Lambda} q(\lambda) p_1(\sigma_J | \lambda) p_2(\sigma_K | \lambda) d\lambda, \quad (19)$$

where the integral runs over all possible values of the variables  $\lambda$ . In order to correspond with our qubit measurements, we consider a case where the first observer makes measurements of the spin projection scaled to  $\pm 1$  along axis A or B, and the second observer makes measurements along axis B or C. The expectation value of the product  $\sigma_J \sigma_K$  of measurements made by the first observer along axis J and the second observer along axis K is denoted by  $\langle \sigma_J \sigma_K \rangle$ . We compute S as in Eq. (11). From Eq. (19),

$$\langle \sigma_J \sigma_K \rangle = \int_{\Lambda} q(\lambda) \langle \sigma_J \rangle_{\lambda,1} \langle \sigma_K \rangle_{\lambda,2} d\lambda, \quad (20)$$

where

$$\langle \sigma_J \rangle_{\lambda,1} = p_1(\sigma_J = 1 | \lambda) - p_1(\sigma_J = -1 | \lambda), \quad (21)$$

and similarly for  $\langle \sigma_K \rangle_{\lambda,2}$ . Both  $\langle \sigma_J \rangle_{\lambda,1}$  and  $\langle \sigma_K \rangle_{\lambda,2}$  must have values between  $-1$  and  $1$ . With the assumption of locality, S in Eq. (11) can be expressed as an integral over  $\lambda$  of  $q(\lambda)$  multiplied by  $S_\lambda$ , where

$$S_\lambda = \langle \sigma_A \rangle_{\lambda,1} [\langle \sigma_B \rangle_{\lambda,2} + \langle \sigma_C \rangle_{\lambda,2}] + \langle \sigma_B \rangle_{\lambda,1} [\langle \sigma_B \rangle_{\lambda,2} - \langle \sigma_C \rangle_{\lambda,2}]. \quad (22)$$

Then still following Brunner *et al.*,<sup>59</sup>

$$S_\lambda \leq | \langle \sigma_A \rangle_{\lambda,1} [ \langle \sigma_B \rangle_{\lambda,2} + \langle \sigma_C \rangle_{\lambda,2} ] | + | \langle \sigma_B \rangle_{\lambda,1} [ \langle \sigma_B \rangle_{\lambda,2} - \langle \sigma_C \rangle_{\lambda,2} ] | , \quad (23)$$

from the triangle inequality. Since the absolute value of the product is the product of the absolute values, and both  $\langle \sigma_A \rangle_{\lambda,1}$  and  $\langle \sigma_B \rangle_{\lambda,1}$  are between  $-1$  and  $1$ , we find

$$S_\lambda \leq | [ \langle \sigma_B \rangle_{\lambda,2} + \langle \sigma_C \rangle_{\lambda,2} ] | + | [ \langle \sigma_B \rangle_{\lambda,2} - \langle \sigma_C \rangle_{\lambda,2} ] | . \quad (24)$$

Then (without loss of generality) assuming that  $1 \geq \langle \sigma_B \rangle_{\lambda,2} \geq \langle \sigma_C \rangle_{\lambda,2} \geq 0$ , it follows that  $S_\lambda$  satisfies  $S_\lambda = 2 \langle \sigma_B \rangle_{\lambda,2} \leq 2$ . Since the distribution  $q(\lambda)$  is normalized, this means that  $S \leq 2$  in any case where locality holds.<sup>59</sup>

We have determined the product  $\langle \sigma_J \sigma_K \rangle$  for a given pair of axes J and K, by taking the combination  $p(00) + p(11) - [ p(01) + p(10) ]$  for runs with those axes. In our calculations, with axes A and B separated by the angle  $\theta$ , and B and C separated by  $\theta'$ , the predicted value of S from Eq. (11) is

$$\begin{aligned} S &= \langle \sigma_A \sigma_B \rangle + \langle \sigma_A \sigma_C \rangle + \langle \sigma_B \sigma_B \rangle - \langle \sigma_B \sigma_C \rangle \leq 2 \\ &= \cos^2(\theta/2) - \sin^2(\theta/2) + \cos^2[(\theta + \theta')/2] - \sin^2[(\theta + \theta')/2] + 1 - \cos^2(\theta'/2) + \sin^2(\theta'/2) \\ &= 1 + \cos(\theta) - \cos(\theta') + \cos(\theta + \theta') . \end{aligned} \quad (25)$$

We have examined cases with  $\theta = \pi/3$  and  $\theta'$  ranging from  $\pi$  to  $2\pi$ . The specific inequality that governs the probabilities in Eq. (10) is valid for these cases, but analogous inequalities break down. For example, the inequality  $p(A^+B^+) + p(A^-B^-) \leq p(B^+C^+) + p(B^-C^-) + p(A^+C^-) + p(A^-C^+)$  is violated for  $\pi < \theta' < 5\pi/3$ . In this same range,  $S > 2$ .

As before, we have used 10 runs with 8192 shots for axes with relative angles of  $\theta$ ,  $\theta'$ , and  $(\theta + \theta')$ , then formed the 1000 combinations generated by these runs, and evaluated the average S value and its standard deviation. The results are listed in Table 4. Figure 9 shows the raw results for the averaged S value and the error-mitigated results, with the mitigation matrix determined

separately, outside of these runs on the ourense<sup>135</sup> quantum computer. The results are plotted as a function of the angle  $\theta'$ . Again, both mitigated results (in green) and raw results (in red) lie along curves that are strikingly well-behaved. There are two exceptions to this pattern, for the error-mitigated results with  $\theta' = 13\pi/8$  or  $41\pi/24$ . In both of these cases, it was necessary to determine  $\langle \sigma_A \sigma_C \rangle$  for a quite small angle of  $\pi/24$  between the A and C axes. After error mitigation, the value of  $\langle \sigma_A \sigma_C \rangle$  exceeded one by approximately 12%. The points plotted in magenta were obtained by capping the correlation  $\langle \sigma_A \sigma_C \rangle$  exactly at one, in the cases where  $\langle \sigma_A \sigma_C \rangle$  would otherwise have exceeded one.

The value of S exceeds 2 for both the raw results and the error-mitigated results, showing that no local hidden-variable theory can be compatible with the runs on the quantum computer, subject to the definition of locality in Eq. (18).<sup>59</sup> In these runs, the maximum S value prior to error mitigation exceeds 2 by 6.27 standard deviations. After error mitigation, the maximum S value exceeds 2 by 12.89 standard deviations. The error-mitigated results for S as a function of the angle  $\theta'$  fall very close to the quantum predictions.

## VI. Summary and conclusions

In this work, we have provided quantitative measures of the essentially quantum character of the qubits on IBM's publicly accessible quantum computers. The inequality in Eq. (10) is a variant of the Bell inequalities suggested by Polkinghorne.<sup>4</sup> This inequality tests whether the spin projections for spin-1/2 particles may *exist* simultaneously along three distinct axes A, B, and C, even though they cannot be measured simultaneously along the three axes. If the spin projections exist simultaneously, then the particles can be classified completely into one of eight disjoint sets, according to whether the spin points up or down along each of the axes. The inequality in Eq. (10) follows directly from this classification. We have found numerous violations of this inequality for the qubits as listed in Table 2 and plotted in Figure 6. We have also found that for a fixed angle  $\theta = \pi/3$  between A and B and a variable angle  $\theta'$  between B and C (with A, B, and C coplanar), the extent of violation as a function of  $\theta'$  follows the quantum mechanical predictions reasonably well in terms of the raw data and quite well in terms of the error-mitigated data, in runs on london.<sup>134</sup> Even without error mitigation, the average differences  $\Delta$  that we have found between  $p(A^+B^+) + p(A^-B^-)$  and the sum  $p(A^+C^+) + p(A^-C^-) + p(B^+C^-) + p(B^-C^+)$  exceed zero by more than 20 standard deviations in runs on vigo<sup>132</sup> and ourense.<sup>135</sup>

The Clauser-Horne-Shimony-Holt inequality<sup>5</sup> in Eq. (11) provides a test of locality. If  $S$  exceeds 2, then a local hidden-variable theory cannot be formulated to match the quantum predictions; in this context, the condition for locality is specified in Eqs. (18) and (19) as proposed by Brunner *et al.*<sup>59</sup> As before, we have found numerous cases in which  $S$  exceeds 2, listed in Table 4 and plotted in Figure 9. With  $\theta = \pi/3$ , the value of  $S$  as a function of  $\theta'$  follows the quantum predictions prior to mitigation and fits the predictions very well after error mitigation. The

maximum value of  $S$  in our runs exceeds 2 by more than 6 standard deviations prior to mitigation and by more than 12 standard deviations after error mitigation.

The accuracy of these results overall was somewhat surprising to us, given the known single-qubit U2 error rates, the C-NOT error rates,<sup>3</sup> and the measurement faults revealed by preparing two qubits in states that should be exclusively  $|00\rangle$ ,  $|01\rangle$ ,  $|10\rangle$ , or  $|11\rangle$ , and observing that all of the other states are typically found in the output. It is noteworthy that the averages of both  $\Delta$  and  $S$  from our runs with 8192 shots show a striking regularity as a function of the angle  $\theta'$ . In our view, this suggests that the remaining faults may be systematic, rather than random. The effects of error mitigation tend to support this view. We have applied error-mitigation matrices that were determined outside of the runs to find  $\Delta$  and  $S$ . The error mitigation matrices were not adapted to the calculations being run, since they were determined without coupling the qubits and without applying a rotation to any qubit (other than complete inversion). The mitigation matrices for burlington,<sup>131</sup> vigo,<sup>132</sup> london,<sup>134</sup> and ourense<sup>135</sup> differ somewhat among themselves, as is apparent from the listing in the Appendix. The mitigation matrices for ourense<sup>135</sup> determined at two separate times did not differ much, however.

The nature of the Bell states themselves has helped to enhance overall accuracy of the determinations of  $\Delta$  and  $S$ . On the whole, we have observed a tendency for the measurement outcome  $|00\rangle$  to be more probable than expected, and for the measurement outcome  $|11\rangle$  to be less probable than expected. Because the analysis relies on sums of probabilities such as  $p(A^+B^+) + p(A^-B^-)$ , some cancellation of errors occurs naturally. Similarly, we have observed asymmetries in the measurement outcomes  $|01\rangle$  and  $|10\rangle$  when they should be equal. The use of combinations such as  $p(B^+C^-) + p(B^-C^+)$  removes the effect of the asymmetries, though it does not completely remove the errors in the probabilities themselves. Designing quantum computing algorithms to



take advantage of Bell-type states may be beneficial in terms of accuracy, when this is possible. Our work offers one benchmark for the accuracy of IBM's publicly available quantum computers, at present.

Bell states provide the basis for one form of quantum cryptography,<sup>139-141</sup> since the no-cloning theorem offers a first line of security for quantum key distribution<sup>142,143</sup> Yet it is possible for three or more observers to share the nonlocality of an entangled pair, with violations of the Bell (CHSH) inequalities found in all of the measurements.<sup>144-147</sup> Experimental confirmations of this possibility have been reported.<sup>148-150</sup> Still, the information that can be gained by an eavesdropper is subject to a tight bound based on the extent of violation of a Bell inequality (Acín).<sup>151</sup> Xu *et al.*<sup>141</sup> have reviewed multiple types of hacking attacks on quantum key distribution, with reference to experimental tests of security measures.

The formation of Bell states between an ancillary qubit and a qubit that is subject to an unknown quantum map permits full characterization of the quantum dynamics.<sup>152-154</sup> Hamiltonian actions on the qubit can be identified; and quantum key distribution methods or quantum repeaters can be verified.<sup>152</sup> The population relaxation time  $T_1$  and the dephasing time  $T_2$  can also be determined.<sup>152</sup> The approach has been generalized to cover two-qubit exchange Hamiltonians, with a pair of ancillary qubits,<sup>153</sup> and to characterize the dynamics when the Bell state is noisy.<sup>154</sup>

Randomness certification<sup>155-157</sup> can be accomplished with Bell states, which also permit extremely dense coding,<sup>158,159</sup> teleportation,<sup>160-163</sup> delayed-choice quantum erasure,<sup>164-166</sup> and entanglement swapping.<sup>167,168</sup> Entangled states of multiple qubits are used in improved methods of error correction.<sup>115-127</sup> Thus the Bell states have considerable utility beyond the demonstration of inherently quantum characteristics, or tests of the accuracy of quantum gates and measurements, as in the current work.

**Author Contributions:** All four co-authors have participated in the software development, investigation, data curation, formal analysis, and validation, as well as parts of the visualization. Katharine Hunt has been responsible for the conceptualization of the project and its methodology, the project administration, supervision, writing, and funding acquisition, as well as the generation and analysis of the results for the CHSH inequalities in Sec. V.

**Conflicts of Interest:** Katharine Hunt became a member of the IBM Quantum Educators Program after this work was largely complete, but this does not present a conflict of interest. The views expressed are those of the authors, and do not reflect the official policy or position of IBM or the IBM Quantum team.

**Acknowledgments:** We gratefully acknowledge the use of IBM Quantum services for this work. This work has been supported in part by the National Science Foundation, through grant CHE-1900399 to Michigan State University (KLCH). We are grateful for support from the Herbert H. and Grace A. Dow Foundation, the Rollin M. Gerstaecker Foundation, and the Charles J. Strosacker Foundation, which provided summer internships and fellowships for David Wang, Aidan Gauthier, and Ashley Siegmund during Summers 2019 and 2020, as well as operational support for the MSU St. Andrews Facility. We thank Guanghan Ma for useful discussions during Summer 2019 and thank Andrew Scheffer for helpful comments about mitigation matrices during Summer 2020. KLCH thanks John Furcean for providing instruction in Python programming to the interns during Summer 2019, and for assistance to the group in installing Anaconda<sup>®</sup>, Jupyter<sup>®</sup>, and Spyder<sup>®</sup> during Summers 2019 and 2020.

## References

- 1 J. S. Bell, *Physics, Physique, Fizika*, 1964, **1**, 195–200.
- 2 J. S. Bell, *Speakable and Unspeakable in Quantum Mechanics*, Cambridge University Press, Cambridge, England, 2004.
- 3 IBM Q Experience® is a trademark of International Business Machines Corporation, registered in many jurisdictions worldwide. See [quantum-computing.ibm.com](http://quantum-computing.ibm.com)
- 4 J. C. Polkinghorne, *The Quantum World*, Princeton University Press, Princeton, NJ, 1986.
- 5 J. F. Clauser, M. A. Horne, A. Shimony and R. A. Holt, *Phys. Rev. Lett.*, 1969, **23**, 880–884.
- 6 A. Einstein, B. Podolsky and N. Rosen, *Phys. Rev.*, 1935, **47**, 777–780.
- 7 R. P. Feynman, *Int. J. Theoretical Phys.*, 1982, **21**, 467–488.
- 8 D. Deutsch, *Proc. R. Soc. (London) A*, 1985, **400**, 97–117.
- 9 D. Deutsch and R. Josza, *Proc. R. Soc. (London) A*, 1992, **439**, 553–558.
- 10 R. Cleve, A. Ekert, C. Macchiavello and M. Mosca, *Proc. R. Soc. (London) A*, 1998, **454**, 339–354.
- 11 S. McArdle, S. Endo, A. Aspuru-Guzik, S. C. Benjamin and X. Yuan, *Rev. Mod. Phys.*, 2020, **92**, 015003.
- 12 Y. Cao, J. Romero, J. P. Olson, M. Degroote, P. D. Johnson, M. Kieferova, I. D. Kivlichan, T. Menke, B. Peropadre, N. P. D. Sawaya, S. Sim, L. Veis and A. Aspuru-Guzik, *Chem. Rev.*, 2019, **119**, 10856.
- 13 S. Kais, S. A. Rice and A. R. Dinner, *Quantum Information and Computation for Chemistry*, *Advan. Chem. Phys.*, **154**, John Wiley & Sons, New York, 2014.
- 14 L. Veis and J. Pittner, *Advan. Chem. Phys.*, 2014, **154**, 107–135.
- 15 M. H. Yung, J. D. Whitfield, S. Boixo, D. G. Tempel and A. Aspuru-Guzik, *Advan. Chem. Phys.*, 2014, **154**, 67–106.
- 16 A. Aspuru-Guzik, R. Lindh and M. Reiher, *ACS Central Science*, 2018, **4**, 144–152.
- 17 I. Kassal, J. D. Whitfield, A. Perdomo-Ortiz, M.-H. Yung and A. Aspuru-Guzik, *Ann. Rev. Phys. Chem.*, 2011, **61**, 185–207.
- 18 P. Jordan and E. Wigner, *Z. Phys.*, 1928, **47**, 631–651.
- 19 S. B. Bravyi and A. Y. Kitaev, *Ann. Phys. (Amsterdam)*, 2002, **298**, 210–226.
- 20 J. T. Seeley, M. J. Richard and P. J. Love, *J. Chem. Phys.*, 2012, **137**, 224109.
- 21 A. Tranter, S. Sofia, J. Seeley, M. Kaicher, J. McClean, R. Babbush, P. V. Coveney, F. Mintert, F. Wilhelm and P. J. Love, *Int. J. Quantum Chem.*, 2015, **115**, 1431–1441.
- 22 A. Tranter, P. J. Love, F. Mintert and P. V. Coveney, *J. Chem. Theory Comp.*, 2018, **14**, 5617–5630.
- 23 H. Havlíček, M. Troyer and J. D. Whitfield, *Phys. Rev. A*, 2017, **95**, 032332.
- 24 F. A. Evangelista, G. K.-L. Chan and G. E. Scuseria, *J. Chem. Phys.*, 2019, **151**, 244112.
- 25 H. F. Trotter, *Proc. Am. Math. Soc.*, 1959, **10**, 545–551.
- 26 I. O. Sokolov, P. K. Barkoutsos, P. J. Ollitrault, D. Greenberg, J. Rice, M. Pistoia, and I. Tavernelli, *J. Chem. Phys.*, 2020, **152**, 124107.
- 27 N. P. Bauman, G. H. Low and K. Kowalski, *J. Chem. Phys.*, 2019, **151**, 234114.
- 28 P. J. J. O’Malley, R. Babbush, I. D. Kivlichan, J. Romero, J. R. McClean, R. Barends, J. Kelly, P. Roushan, A. Tranter, N. Ding, B. Campbell, Y. Chen, Z. Chen, B. Chiaro, A. Dunsworth, A. G. Fowler, E. Jeffrey, E. Lucero, A. Megrant, J. Y. Mutus, M. Neeley, C. Neill, C. Quintant, D. Sank, A. Vainsencher, J. Wenner, T. C. White, P. V. Coveney, P. J. Love, H. Neven, A. Aspuru-Guzik and J. M. Martinis, *Phys. Rev. X*, 2016, **6**, 031007.

- 29 K. Setia and J. D. Whitfield, *J. Chem. Phys.*, 2018, **148**, 164104.
- 30 J. I. Colless, V. V. Ramasesh, D. Dahlen, M. S. Blok, M. E. Kimchi-Schwartz, J. R. McClean, J. Carter, W. A. de Jong and I. Siddiqi, *Phys. Rev. X*, 2018, **8**, 011021.
- 31 A. Kandala, A. Mezzacapo, K. Temme, M. Takita, M. Brink, J. M. Chow and J. M. Gambetta, *Nature*, 2017, **549**, 242–246.
- 32 M. Otten and S. K. Gray, *NPJ Quantum Information*, 2019, **5**, 11.
- 33 Y. Wang, F. Dolde, J. Biamonte, R. Babbush, V. Bergholm, S. Yang, I. Jakobi, P. Neumann, A. Aspuru-Guzik, J. D. Whitfield and J. Wrachtrup, *ACS Nano*, 2015, **9**, 7769–7774.
- 34 S. E. Smart and D. A. Mazziotti, *Phys. Rev. A*, 2019, **100**, 022517.
- 35 J. Romero, R. Babbush, J. R. McClean, C. Hempel, P. J. Love and A. Aspuru-Guzik, *Quantum Sci. Technol.*, 2019, **4**, 014008.
- 36 N. H. Stair, R. Huang and F. A. Evangelista, *J. Chem. Theory and Comput.*, 2020, **16**, 2236–2245.
- 37 N. Yunseong, J.-S. Chen, N. C. Pienti, K. Wright, C. Delaney, D. Maslov, K. R. Brown, S. Allen, J. M. Amini, J. Apisdorf, K. M. Beck, A. Blinov, V. Chaplin, M. Chmielewski, C. Collins, S. Debnath, K. M. Hudek, A. M. Ducore, M. Keesan, S. M. Kreikemeier, J. Mizrahi, P. Solomon, M. Williams, J. D. Wong-Campos, D. Moehring, C. Monroe and J. Kim, *NPJ Quantum Information*, 2020, **6**, 33.
- 38 H. Wang, S. Kais, A. Aspuru-Guzik and M. R. Hoffmann, *Phys. Chem. Chem. Phys.*, 2008, **10**, 5388–5393.
- 39 I. G. Ryabinkin, T.-C. Yen, S. N. Genin and A. F. Izmaylov, *J. Chem. Theory Comput.*, 2018, **14**, 6317–6326.
- 40 R. Xia and S. Kais, *Entropy*, 2020, **22**, 828.
- 41 S. E. Smart, D. Schuster and D. A. Mazziotti, *Commun. Phys.*, 2019, **2**, 11.
- 42 R. E. Borland and K. Dennis, *J. Phys. B: Atomic, Molecular and Optical Phys.*, 1972, **5**, 7–15.
- 43 M. Altunbulak and A. Klyachko, *Commun. Math. Phys.*, 2008, **282**, 287–322.
- 44 M. Walter, B. Doran, D. Gross, and M. Christandl, *Science*, 2012, **340**, 1205–1208.
- 45 A. Higuchi, A. Sudbery and J. Szulc, *Phys. Rev. Lett.*, 2003, **90**, 107902.
- 46 M. Sisodia, *Quantum Information Processing*, 2020, **19**, 215.
- 47 E. Huffman and A. Mizel, *Phys. Rev. A*, 2017, **95**, 032131.
- 48 A. J. Leggett and A. Garg, *Phys. Rev. Lett.*, 1985, **54**, 857–860.
- 49 I. Hamamura, *Phys. Lett. A*, 2018, **382**, 2573–2577.
- 50 M. B. Pozzobom and J. Maziero, *Quantum Information Processing*, 2019, **18**, 142.
- 51 D. Alsina and J. I. Latorre, *Phys. Rev. A*, 2016, **94**, 012314.
- 52 N. D. Mermin, *Phys. Rev. Lett.*, 1990, **65**, 1838–1840.
- 53 M. Ansmann, H. Wang, R. C. Bialczak, M. Hofheinz, E. Lucero, M. Neeley, A. D. O’Connell, D. Sank, M. Weides, J. Wenner, A. N. Cleland and J. M. Martinis, *Nature*, 2009, **461**, 504–506.
- 54 J. Koch, T. M. Yu, J. Gambetta, A. A. Houck, D. I. Schuster, J. Majer, A. Blais, M. H. Devoret, S. M. Girvin and R. J. Schoelkopf, *Phys. Rev. A*, 2007, **76**, 042319.
- 55 J. A. Schreier, A. A. Houck, J. Koch, D. I. Schuster, B. R. Johnson, J. M. Chow, J. M. Gambetta, J. Majer, L. Frunzio, M. H. Devoret, S. M. Girvin and R. J. Schoelkopf, *Phys. Rev. B*, 2008, **77** 180502(R).
- 56 A. Ekert, P. M. Hayden and H. Inamori, *Coherent Matter Waves*, Les Houches Summer School Session, 2001, **72**, 663–701.

- 57 IBM's qiskit<sup>®</sup> is a trademark of International Business Machines Corporation, registered in many jurisdictions worldwide. See qiskit.org.
- 58 F. Bloch, *Phys. Rev.*, 1946, **70**, 460–474.
- 59 N. Brunner, D. Cavalcanti, S. Pironio, V. Scarani and S. Wehner, *Rev. Mod. Phys.*, 2014, **86**, 419–478.
- 60 S. J. Freedman and J. F. Clauser, *Phys. Rev. Lett.*, 1972, **28**, 938–941.
- 61 M. Giustina, A. Mech, S. Ramelow, B. Wittmann, J. Kofler, J. Beyer, A. Lita, B. Calkins, T. Gerrits, S. Nam, R. Ursin and A. Zeilinger, *Nature*, 2013, **497**, 227–230.
- 62 J. A. Larsson, M. Giustina, J. Kofler, B. Wittmann, R. Ursin and S. Ramelow, *Phys. Rev. A*, 2014, **90**, 032107.
- 63 P. M. Pearle, *Phys. Rev. D*, 1970, **2**, 1418–1425.
- 64 A. Garg and N. D. Mermin, *Phys. Rev. D*, 1987, **35**, 3831–3835.
- 65 P. H. Eberhard, *Phys. Rev. A*, 1993, **47**, R747–R750.
- 66 K. Sen, S. Das and U. Sen, *Phys. Rev. A*, 2019, **100**, 062333.
- 67 J. Barrett, D. Collins, L. Hardy, A. Kent and S. Popescu, *Phys. Rev. A*, 2002, **66**, 042111.
- 68 M.-H. Li, C. Wu, Y. Zhang, W.-Z. Liu, B. Bai, Y. Liu, W. Zhang, Q. Zhao, H. Li, Z. Wang, L. You, W. J. Munro, J. Yin, J. Zhang, C.-Z. Peng, X. Ma, Q. Zhang, J. Fan and J.-W. Pan, *Phys. Rev. Lett.*, 2018, **121**, 080404.
- 69 K. F. Pal and T. Vertesi, *Phys. Rev. A*, 2015, **92**, 022103.
- 70 B. G. Christensen, K. T. McCusker, J. B. Altepeter, B. Calkins, T. Gerrits, A. E. Lita, A. Miller, L. K. Shalm, Y. Zhang, S. W. Nam, N. Brunner, C. C. W. Lim, N. Gisin and P. G. Kwiat, *Phys. Rev. Lett.*, 2013, **111**, 130406.
- 71 E. S. Fry and R. C. Thompson, *Phys. Rev. Lett.*, 1976, **37**, 465–468.
- 72 A. Aspect, P. Grangier and G. Roger, *Phys. Rev. Lett.*, 1981, **47**, 460–463.
- 73 A. Aspect, P. Grangier and G. Roger, *Phys. Rev. Lett.*, 1982, **49**, 91–94.
- 74 A. Aspect, J. Dalibard and G. Roger, *Phys. Rev. Lett.*, 1982, **49**, 1804–1807.
- 75 W. Tittel, J. Brendel, H. Zbinden and N. Gisin, *Phys. Rev. Lett.*, 1998, **81**, 3563–3566.
- 76 A. Fedrizzi, R. Ursin, T. Herbst, M. Nespoli, R. Prevedel, T. Scheidl, F. Tiefenbacher, T. Jennewein and A. Zeilinger, *Nat. Phys.*, 2009, **5**, 389–392.
- 77 G. Weihs, T. Jennewein, C. Simon, H. Weinfurter and A. Zeilinger, *Phys. Rev. Lett.*, 1998, **81**, 5039–5043.
- 78 J. Handsteiner, A. S. Friedman, D. Rauch, J. Gallicchio, B. Liu, H. Hosp, J. Kofler, D. Bricher, M. Fink, C. Leung, A. Mark, H. T. Nguyen, I. Sanders, F. Steinlechner, R. Ursin, S. Wengerowsky, A. H. Guth, D. I. Kaiser, T. Scheidl and A. Zeilinger, *Phys. Rev. Lett.*, 2017, **118**, 060401.
- 79 B. Hensen, H. Bernien, A. E. Dréau, A. Reiserer, N. Kalb, M. S. Blok, J. Ruitenberg, R. F. L. Vermeulen, R. N. Schouten, C. Abellán, W. Amaya, V. Pruneri, M. W. Mitchell, M. Markham, D. J. Twitchen, D. Elkouss, S. Wehner, T. H. Taminiau and R. Hanson, *Nature*, 2015, **526**, 682–686.
- 80 B. Hensen, N. Kalb, M. S. Blok, A. E. Dréau, A. Reiserer, R. F. L. Vermeulen, R. N. Schouten, M. Markham, D. J. Twitchen, K. Goodenough, D. Elkouss, S. Wehner, T. H. Taminiau and R. Hanson, *Sci. Rep.*, 2016, **6**, 30289.
- 81 J. P. Dehollain, S. Simmons, J. T. Muhonen, R. Kalra, A. Laucht, F. Hudson, K. M. Itoh, D. N. Jamieson, J. C. McCallum, A. S. Dzurak and A. Morello, *Nature Nanotechnology*, 2016, **11**, 242–246.
- 82 I. Marinković, A. Wallucks, R. Riedinger, S. Hong, M. Aspelmeyer and S. Gröblacher, *Phys.*

- Rev. Lett.*, 2018, **121**, 220404.
- 83 M. A. Rowe, D. Kielpinski, V. Meyer, C. A. Sackett, W. M. Itano, C. Monroe and D. J. Wineland, *Nature*, 2001, **409**, 791–794.
- 84 D. N. Matsukevich, P. Maunz, D. L. Moehring, S. Olmschenk and C. Monroe, *Phys. Rev. Lett.*, 2008, **100**, 150404.
- 85 J. Hofmann, M. Krug, N. Ortegel, L. Gérard, M. Weber, W. Rosenfeld and H. Weinfurter, *Science*, 2012, **337**, 72–75.
- 86 C. Aucher, C.-K. Chou, T. W. Noel and B. B. Blinov, *J. Opt. Soc. Am. B—Opt. Phys.*, 2014, **31**, 1568–1572.
- 87 T. Scheidl, R. Ursin, J. Kofler, S. Ramelow, X.-S. Ma, T. Herbst, L. Ratschbacher, A. Fedrizzi, N. K. Langford, T. Jennewein and A. Zeilinger, *Proc. Natl. Acad. Sci. USA*, 2010, **107**, 19708–19713.
- 88 M. Giustina, M. A. M. Versteegh, S. Wengerowsky, J. Handsteiner, A. Hochrainer, K. Phelan, F. Steinlechner, J. Kofler, J. A. Larsson, C. Abellan, W. Amaya, V. Pruneri, M. W. Mitchell, J. Beyer, T. Gerrits, A. E. Lita, L. K. Shalm, S. W. Nam, T. Scheidl, R. Ursin, B. Wittmann and A. Zeilinger, *Phys. Rev. Lett.*, 2015, **115**, 250401.
- 89 B. G. Christensen, Y.-C. Liang, N. Brunner, N. Gisin and P. G. Kwiat, *Phys. Rev. X*, 2015, **5**, 041052.
- 90 D. Greenberger, M. Horne and A. Zeilinger, *Bell's Theorem, Quantum Theory, and Conceptions of the Universe*, Kluwer Academic, Dordrecht, 1989, p. 73.
- 91 J.-W. Pan, D. Bouwmeester, M. Daniell, H. Weinfurter and A. Zeilinger, *Nature*, 2000, **403**, 515–519.
- 92 J. Lavoie, R. Kaltenbaek and K. Resch, *New J. Phys.*, 2009, **11**, 073051.
- 93 W. Dür, G. Vidal and J. I. Cirac, *Phys. Rev. A*, 2000, **62**, 062314.
- 94 M. Eibl, N. Kiesel, M. Bourennane, C. Kurtsiefer, and H. Weinfurter, *Phys. Rev. Lett.*, 2004, **92**, 077901.
- 95 N. J. Cerf and C. Adami, *Phys. Rev. A*, 1997, **55**, 3371–3374.
- 96 C. Tsallis, S. Lloyd and M. Baranger, *Phys. Rev. A*, 2001, **63**, 042104.
- 97 B. M. Terhal, *Theor. Comp. Sci.*, 2002, **287**, 313–335.
- 98 F. A. Bovino, G. Castagnoli, A. Ekert, P. Horodecki, C. M. Alves and A. V. Sergienko, *Phys. Rev. Lett.*, 2005, **95**, 240407.
- 99 F. A. Bovino, *Int. J. Theor. Phys.*, 2008, **47**, 2148–2157.
- 100 R. Horodecki, P. Horodecki, M. Horodecki and K. Horodecki, *Rev. Mod. Phys.*, 2009, **81**, 865–942.
- 101 R. Chaves and T. Fritz, *Phys. Rev. A*, 2012, **85**, 032113.
- 102 R. Chaves, *Phys. Rev. A*, 2013, **87**, 022102.
- 103 Z.-B. Chen, Y. Fu and Y.-K. Zhao, *Phys. Rev. A*, 2014, **90**, 022124.
- 104 A. E. Rastegin, *Ann. Phys.*, 2015, **355**, 241–257.
- 105 M. Wajs, P. Kurzyński and D. Kaszlikowski, *Phys. Rev. A*, 2015, **91**, 012114; *Phys. Rev. A*, 2015, **91**, 019903.
- 106 R. Chaves and C. Budroni, *Phys. Rev. Lett.*, 2016, **116**, 240501.
- 107 L.-Z. Cao, J.-Q. Zhao, X. Liu, Y. Yang, Y.-D. Li, X.-Q. Wang, Z.-B. Chen and H.-X. Lu, *Sci. Rep.*, 2016, **6**, 23758.
- 108 N. Miklin, A. A. Abbott, C. Branciard, R. Chaves and C. Budroni, *New J. Phys.*, 2017, **19**, 113041.
- 109 T. Gläfle, D. Gross and R. Chaves, *J. Phys. A—Mathematical and Theoretical*, 2018, **51**,

- 484002.
- 110 A. Carmi and E. Cohen, *Entropy*, 2018, **20**, 500.
- 111 A. Bednorz, W. Bednorz and W. Belzig, *Phys. Rev. A*, 2014, **89**, 022125.
- 112 M. Eibl, S. Gaertner, M. Bourennane, C. Kurtsiefer, M. Żukowski and H. Weinfurter, *Phys. Rev. Lett.*, 2003, **90**, 200403.
- 113 Z. Zhao, T. Yang, Y.-A. Chen, A.-N. Zhang, M. Żukowski and J.-W. Pan, *Phys. Rev. Lett.*, 2003, **91**, 180401.
- 114 P. Walther, M. Aspelmayer, K. J. Resch and A. Zeilinger, *Phys. Rev. Lett.*, 2005, **95**, 020403.
- 115 J. R. Wootton, *J. Mod. Optics*, 2012, **59**, 1717–1738.
- 116 J. Roffe, *Contemporary Phys.*, 2019, **60**, 226–245.
- 117 J. R. Wootton, *Quantum Sci. Tech.*, 2020, **5**, 044004.
- 118 P. W. Shor, *Phys. Rev. A*, 1995, **52**, R2493–R2496.
- 119 A. Steane, *Proc. R. Soc. (London). A*, 1996, **452**, 2551–2577.
- 120 R. Laflamme, C. Miquel, J. P. Paz and W. H. Zurek, *Phys. Rev. Lett.*, 1996, **77**, 198–201.
- 121 C. H. Bennett, D. P. DiVincenzo, J. A. Smolin and W. K. Wootters, *Phys. Rev. A*, 1996, **54**, 3824–3851.
- 122 R. Raussendorf, *Phil. Trans. R. Soc. A*, 2012, **370**, 4541–4565.
- 123 S. J. Devitt, W. J. Munro and K. Nemoto, *Rep. Prog. Phys.*, 2013, **76**, 076001.
- 124 D. A. Lidar and T. A. Brun, *Quantum Error Correction*, Cambridge University Press, Cambridge, England, 2013.
- 125 B. M. Terhal, *Rev. Mod. Phys.*, 2015, **87**, 307.
- 126 A. Y. Kitaev, *Russian Math. Surveys*, 1997, **52**, 1191–1249.
- 127 R. Laflamme, C. Miquel, J. P. Paz and W. H. Zurek, *Phys. Rev. Lett.*, 1996, **77**, 198–201.
- 128 A. R. Calderbank and P. W. Shor, *Phys. Rev. A*, 1996, **54**, 1098–1105.
- 129 T. Brun, I. Devetak and M.-H. Hsieh, *Science*, 2006, **314**, 436–439.
- 130 R. J. Harris, N. A. McMahon, G. K. Brennen and T. M. Stace, *Phys. Rev. A*, 2018, **98**, 052301.
- 131 ibmq\_burlington v1.1.4, IBM Quantum team. Retrieved from <https://quantum-computing.ibm.com> (2020).
- 132 ibmq\_vigo v1.2.1, IBM Quantum team. Retrieved from <https://quantum-computing.ibm.com> (2020).
- 133 ibmq\_essex v1.0.2, IBM Quantum team. Retrieved from <https://quantum-computing.ibm.com> (2020).
- 134 ibmq\_london v1.1.3, IBM Quantum team. Retrieved from <https://quantum-computing.ibm.com> (2020).
- 135 ibmq\_ourense v1.2.0, IBM Quantum team. Retrieved from <https://quantum-computing.ibm.com> (2020).
- 136 E. Merzbacher, *Quantum Mechanics*, John Wiley & Sons, New York, NY, 1961.
- 137 ibmq\_qasm\_simulator v0.1.547, IBM Quantum team. Retrieved from <https://quantum-computing.ibm.com> (2020).
- 138 ibmq\_16\_melbourne v2.3.1, IBM Quantum team. Retrieved from <https://quantum-computing.ibm.com> (2020).
- 139 A. Ekert, *Phys. Rev. Lett.*, 1991, **67**, 661–663.
- 140 N. Gisin, G. Ribordy, W. Tittel and H. Zbinden, *Rev. Mod. Phys.*, 2002, **74**, 145.
- 141 F. Xu, X. Ma, Q. Zhang, H.-K. Lo and J.-W. Pan, *Rev. Mod. Phys.*, 2020, **92**, 025002.
- 142 D. Dieks, *Phys. Lett. A*, 1982, **92**, 271–272.

- 143 W. K. Wootters and W. H. Zurek, *Nature*, 1982, **299**, 802–803.
- 144 R. Silva, N. Gisin, Y. Guryanova and S. Popescu, *Phys. Rev. Lett.*, 2015, **114**, 250401.
- 145 D. Das, A. Ghosal, S. Sasmal, S. Mal and A. S. Majumdar, *Phys. Rev. A*, 2019, **99**, 022305.
- 146 P. J. Brown and R. Colbeck, *Phys. Rev. Lett.* 2020, **125**, 090401.
- 147 A. G. Maity, D. Das, A. Ghosal, A. Roy and A. S. Majumdar, *Phys. Rev. A*, 2020, **101**, 042340.
- 148 M. Schiavon, L. Calderaro, M. Pittaluga, G. Vallone and P. Villoresi, *Quantum Sci. Tech.*, 2017, **2**, 015010.
- 149 M.-J. Hu, Z.-Y. Zhou, X.-M. Hu, C.-F. Li, G.-C. Guo and Y.-S. Zhang, *NPJ Quantum Information*, 2018, **4**, 63.
- 150 G. Foletto, L. Calderaro, A. Tavakoli, M. Schiavon, F. Picciariello, A. Cabello, P. Villoresi and G. Vallone, *Phys. Rev. Applied*, 2020, **13**, 044008; *Phys. Rev. Applied*, 2020, **13**, 069902.
- 151 A. Acín, N. Brunner, N. Gisin, S. Massar, S. Pironio and V. Scarani, *Phys. Rev. Lett.*, 2007, **98**, 230501.
- 152 M. Mohseni and D. Lidar, *Phys. Rev. Lett.* 2006, **97**, 170501.
- 153 M. Mohseni, A. T. Rezakhani, J. T. Barreiro, P. G. Kwiat and A. Aspuru-Guzik, *Phys. Rev. A*, 2010, **81**, 032102.
- 154 M. Mohseni, A. Rezakhani and A. Aspuru-Guzik, *Phys. Rev. A*, 2008, **77**, 042320.
- 155 S. Pironio, A. Acín, S. Massar, A. Boyer de la Giroday, D. N. Matsukevich, P. Maunz, S. Olmschenk, D. Hayes, L. Luo, T. A. Manning and C. Monroe, *Nature*, 2010, **464**, 1021–1024.
- 156 A. C. Martínez, A. Solis, R. D. H. Rojas, A. B. U'Ren, J. G. Hirsch and I. P. Castillo, *Entropy*, 2018, **20**, 886.
- 157 Y. Zhang, E. Knill and P. Bierhorst, *Phys. Rev. A*, 2018, **98**, 040304(R).
- 158 C. H. Bennett and S. J. Wiesner, *Phys. Rev. Lett.*, 1992, **69**, 2881–2884.
- 159 X.-H. Li and S. Ghose, *Phys. Rev. A*, 2017, **96**, 020303.
- 160 C. H. Bennett, G. Brassard, C. Crépeau, R. Jozsa, A. Peres and W. K. Wootters, *Phys. Rev. Lett.*, 1993, **70**, 1895–1899.
- 161 D. Bouwmeester, J.-W. Pan, K. Mattle, M. Eibl, H. Weinfurter and A. Zeilinger, *Nature*, 1997, **390**, 575–579.
- 162 J.-G. Ren, P. Xu, H.-L. Yong, L. Zhang, S.-K. Liao, J. Yin, W.-Y. Liu, W.-Q. Cai, M. Yang, L. Li, K.-X. Yang, X. Han, Y.-Q. Yao, J. Li, H.-Y. Wu, S. Wan, L. Liu, D.-Q. Liu, Y.-W. Kuang, Z.-P. He, P. Shang, C. Guo, R.-H. Zheng, K. Tian, Z.-C. Zhu, N.-L. Liu, C.-Y. Lu, R. Shu, Y.-A. Chen, C.-Z. Peng, J.-Y. Wang and J.-W. Pan, *Nature*, 2017, **549**, 70–73.
- 163 E. Olofsson, P. Samuelsson, N. Brunner and P. P. Potts, *Phys. Rev. B*, 2020, **101**, 195403.
- 164 H. F. Wang and S. Kais, *Chem. Phys. Lett.*, 2006, **421**, 338–342.
- 165 Y. H. Kim, R. Yu, S. P. Kulik, Y. Shih, and M. O. Scully, *Phys. Rev. Lett.*, 2000, **84**, 1–5.
- 166 J. R. Glick and C. Adami, *Phys. Rev. A*, 2017, **95**, 012105.
- 167 B. Yurke and D. Stoler, *Phys. Rev. A*, 1992, **46**, 2229–2234.
- 168 M. Zukowski, A. Zeilinger, M. A. Horne and A. K. Ekert, *Phys. Rev. Lett.*, 1993, **71**, 4287–4290.



**Appendix: External mitigation matrices  $M^{-1}$  used in this work**

The mitigation matrices determined outside the runs on the quantum computers are listed below. We have used the method of construction described in the qiskit documentation<sup>57</sup> (see Sec. III). Matrices that are closer to the identity indicate more accurate operation of the quantum computer. These matrices do not remain stable over long periods. However, the two mitigation matrices for ourense<sup>135</sup> were determined nine days apart, and they differ from each other less than they differ from the other matrices.

burlington<sup>131</sup>

$$M^{-1} = \begin{pmatrix} 1.074988 & -0.124294 & -0.217828 & -0.012518 \\ -0.024451 & 1.165339 & 0.001658 & -0.207666 \\ -0.033282 & 0.001876 & 1.237703 & -0.128352 \\ -0.017255 & -0.042921 & -0.021520 & 1.348218 \end{pmatrix}$$

london<sup>134</sup>

$$M^{-1} = \begin{pmatrix} 1.016556 & -0.076543 & -0.046868 & 0.004441 \\ -0.006517 & 1.092766 & -0.000025 & -0.055147 \\ -0.009573 & 0.000386 & 1.052127 & -0.064562 \\ -0.000476 & -0.016598 & -0.005234 & 1.115267 \end{pmatrix}$$

vigo<sup>132</sup>

$$M^{-1} = \begin{pmatrix} 1.010999 & -0.029718 & -0.025551 & 0.000636 \\ -0.005768 & 1.036088 & -0.000118 & -0.026499 \\ -0.005252 & 0.000215 & 1.033087 & -0.033973 \\ 0.000021 & -0.006575 & -0.007418 & 1.059824 \end{pmatrix}$$

ourense<sup>135</sup>

$$M^{-1} = \begin{pmatrix} 1.034861 & -0.029335 & -0.034065 & 0.000811 \\ -0.013127 & 1.050248 & 0.000270 & -0.037341 \\ -0.021839 & 0.000571 & 1.047827 & -0.041142 \\ -0.000105 & -0.021485 & -0.014032 & 1.077683 \end{pmatrix}$$

Second set of runs on ourense<sup>135</sup>

$$M^{-1} = \begin{pmatrix} 1.032876 & -0.028240 & -0.036447 & 0.000685 \\ -0.012984 & 1.049636 & 0.000263 & -0.042541 \\ -0.020000 & 0.000390 & 1.050376 & -0.029087 \\ -0.000098 & -0.021775 & -0.014192 & 1.070943 \end{pmatrix}$$

**Table 1.** Average values of  $\Delta \equiv p(A^+B^+) + p(A^-B^-) - p(A^+C^+) - p(A^-C^-) - p(B^+C^-) - p(B^-C^+)$  and the standard deviations  $\sigma$  from 1000 combinations of runs for each set of angles on the qasm simulator.<sup>137</sup> Axes A, B, and C are co-planar. Positive values of  $\Delta$  reflect inherently non-classical behavior. Angles  $(\theta + \theta')$  larger than  $\pi$  have been replaced by  $2\pi - (\theta + \theta')$ , which should give identical values of  $\Delta$ , based on quantum mechanical calculations.

A, B angle	B, C angle	A, C angle	$\Delta$	$\sigma$
$\pi/3$	0	$\pi/3$	-0.00204	0.00624
$\pi/3$	$\pi/24$	$3\pi/8$	0.04992	0.00697
$\pi/3$	$\pi/12$	$5\pi/12$	0.10110	0.00620
$\pi/3$	$\pi/8$	$11\pi/24$	0.14510	0.00792
$\pi/3$	$\pi/6$	$\pi/2$	0.17840	0.00750
$\pi/3$	$5\pi/24$	$13\pi/24$	0.21052	0.00764
$\pi/3$	$\pi/4$	$7\pi/12$	0.23295	0.00768
$\pi/3$	$7\pi/24$	$5\pi/8$	0.24640	0.00932
$\pi/3$	$\pi/3$	$2\pi/3$	0.24575	0.00875
$\pi/3$	$3\pi/8$	$17\pi/24$	0.24301	0.00860
$\pi/3$	$5\pi/12$	$3\pi/4$	0.23010	0.00711
$\pi/3$	$11\pi/24$	$19\pi/24$	0.21096	0.00857
$\pi/3$	$\pi/2$	$5\pi/6$	0.18169	0.00723
$\pi/3$	$13\pi/24$	$7\pi/8$	0.14314	0.00796
$\pi/3$	$7\pi/12$	$11\pi/12$	0.09943	0.00713
$\pi/3$	$5\pi/8$	$23\pi/24$	0.05025	0.00808
$\pi/3$	$2\pi/3$	$\pi$	-0.00175	0.00526
$\pi/3$	$17\pi/24$	$25\pi/24 \rightarrow 23\pi/24$	-0.05870	0.00650
$\pi/3$	$3\pi/4$	$13\pi/12 \rightarrow 11\pi/12$	-0.12275	0.00565
$\pi/3$	$19\pi/24$	$9\pi/8 \rightarrow 7\pi/8$	-0.18771	0.00636
$\pi/3$	$5\pi/6$	$7\pi/6 \rightarrow 5\pi/6$	-0.25250	0.00543
$\pi/3$	$7\pi/8$	$29\pi/24 \rightarrow 19\pi/24$	-0.31733	0.00633
$\pi/3$	$11\pi/12$	$5\pi/4 \rightarrow 3\pi/4$	-0.38230	0.00558
$\pi/3$	$23\pi/24$	$31\pi/24 \rightarrow 17\pi/24$	-0.44634	0.00637
$\pi/3$	$\pi$	$4\pi/3 \rightarrow 2\pi/3$	-0.50317	0.00534

**Table 2.** Average values of  $\Delta \equiv p(A^+B^+) + p(A^-B^-) - p(A^+C^+) - p(A^-C^-) - p(B^+C^-) - p(B^-C^+)$  and standard deviations  $\sigma$  from 1000 combinations of runs for each set of angles on london.<sup>134</sup> Values of  $\Delta$  and  $\sigma$  have been obtained with and without error mitigation by a filtering matrix. Values after mitigation are indicated by asterisks. The angle between axes A and B is fixed at  $\pi/3$ .

B, C angle	A, C angle	$\Delta$	$\sigma$	$\Delta^*$	$\sigma^*$
0	$\pi/3$	-0.04928	0.01398	0.01137	0.01636
$\pi/24$	$3\pi/8$	-0.01705	0.00925	0.06220	0.00901
$\pi/12$	$5\pi/12$	0.02378	0.01061	0.09506	0.01217
$\pi/8$	$11\pi/24$	0.06062	0.00907	0.13719	0.01030
$\pi/6$	$\pi/2$	0.08612	0.00876	0.16118	0.00960
$5\pi/24$	$13\pi/24$	0.11292	0.00989	0.19749	0.01142
$\pi/4$	$7\pi/12$	0.11873	0.00909	0.20128	0.01015
$7\pi/24$	$5\pi/8$	0.13140	0.00997	0.21799	0.01137
$\pi/3$	$2\pi/3$	0.13216	0.01426	0.21918	0.01666
$3\pi/8$	$17\pi/24$	0.13054	0.00908	0.21773	0.01024
$5\pi/12$	$3\pi/4$	0.11716	0.01087	0.20242	0.01245
$11\pi/24$	$19\pi/24$	0.10077	0.00941	0.18361	0.01072
$\pi/2$	$5\pi/6$	0.07609	0.00877	0.15601	0.01003
$13\pi/24$	$7\pi/8$	0.04293	0.00997	0.11746	0.01158
$7\pi/12$	$11\pi/12$	-0.00054	0.00857	0.06787	0.00970
$5\pi/8$	$23\pi/24$	-0.04190	0.00986	0.02080	0.01125
$2\pi/3$	$\pi$	-0.09227	0.00850	-0.03678	0.00955
$17\pi/24$	$25\pi/24 \rightarrow 23\pi/24$	-0.13341	0.00881	-0.08408	0.00991
$3\pi/4$	$13\pi/12 \rightarrow 11\pi/12$	-0.18961	0.00805	-0.14849	0.00908
$19\pi/24$	$9\pi/8 \rightarrow 7\pi/8$	-0.23955	0.00895	-0.20580	0.01015
$5\pi/6$	$7\pi/6 \rightarrow 5\pi/6$	-0.29490	0.00843	-0.26892	0.00954
$7\pi/8$	$29\pi/24 \rightarrow 19\pi/24$	-0.35024	0.00895	-0.33204	0.01015
$11\pi/12$	$5\pi/4 \rightarrow 3\pi/4$	-0.40019	0.00805	-0.38935	0.00908
$23\pi/24$	$31\pi/24 \rightarrow 17\pi/24$	-0.45638	0.00881	-0.45376	0.00991
$\pi$	$4\pi/3 \rightarrow 2\pi/3$	-0.49752	0.00850	-0.50106	0.00955

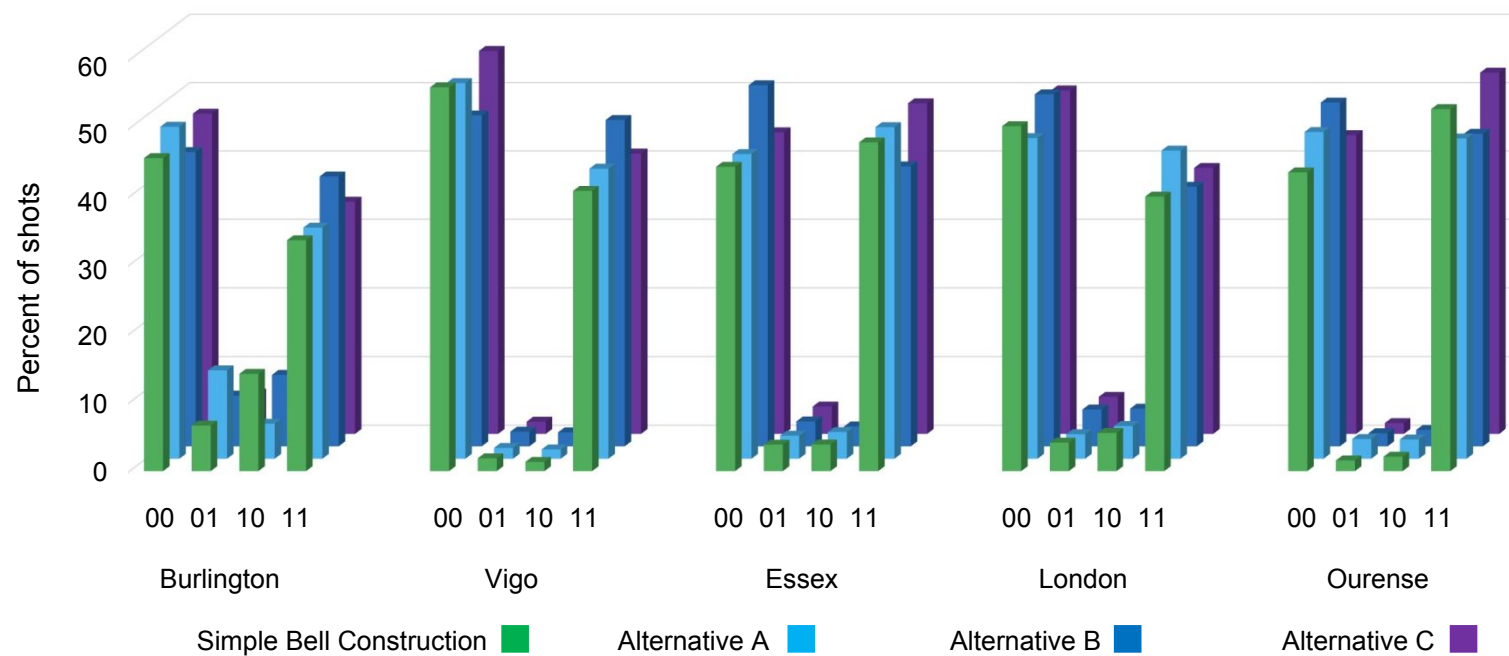
**Table 3.** Comparisons of probabilities for spins to be aligned or opposed for angle pairs that should give identical results. Averages of 10 runs at each angle on ourense<sup>135</sup> and vigo,<sup>132</sup> without mitigation. Results from the ibmq qasm simulator<sup>137</sup> (sim) are shown for comparison. Results for  $\pi/24$  on ourense<sup>135</sup> on the first line were obtained nine days before the corresponding results on the second line.

ourense <sup>135</sup>						
Angle	$p(A^+B^+) + p(A^-B^-)$	Quantum value	$p(A^+B^-) + p(A^-B^+)$	Quantum value	$p(A^+B^+) - p(A^-B^-)$	$p(A^+B^-) - p(A^-B^+)$
$\pi/24$	0.91895	0.99572	0.08106	0.00428	0.04714	0.00676
$\pi/24$	0.87383	0.99572	0.12617	0.00428	0.09192	0.06802
$47\pi/24$	0.86759	0.99572	0.13241	0.00428	0.05956	0.10260
$\pi/2$	0.51417	0.50000	0.48583	0.50000	0.18151	-0.04498
$3\pi/2$	0.48923	0.50000	0.51077	0.50000	-0.02908	0.17791
$23\pi/24$	0.13297	0.00428	0.86703	0.99572	0.11423	0.04681
$25\pi/24$	0.13004	0.00428	0.86996	0.99572	0.08038	0.07304
vigo <sup>132</sup>						
Angle	$p(A^+B^+) + p(A^-B^-)$	Quantum value	$p(A^+B^-) + p(A^-B^+)$	Quantum value	$p(A^+B^+) - p(A^-B^-)$	$p(A^+B^-) - p(A^-B^+)$
$\pi/24$	0.95260	0.99572	0.04740	0.00428	0.08825	-0.01510
$47\pi/24$	0.95238	0.99572	0.04762	0.00428	0.08292	-0.00868
$\pi/2$	0.49243	0.50000	0.50757	0.50000	0.07756	-0.00325
$3\pi/2$	0.51530	0.50000	0.48471	0.50000	0.03676	0.03519
$23\pi/24$	0.04830	0.00428	0.95170	0.99572	0.03353	0.03255
$25\pi/24$	0.04588	0.00428	0.95413	0.99572	0.02695	0.04814

$\sin^{137}$						
Angle	$p(A^+B^+) + p(A^-B^-)$	Quantum value	$p(A^+B^-) + p(A^-B^+)$	Quantum value	$p(A^+B^+) - p(A^-B^-)$	$p(A^+B^-) - p(A^-B^+)$
$\pi/24$	0.99596	0.99572	0.00405	0.00428	0.00626	-0.00003
$47\pi/24$	0.99679	0.99572	0.00421	0.00428	-0.00299	-0.00006
$\pi/2$	0.49575	0.50000	0.50425	0.50000	-0.00059	0.00262
$3\pi/2$	0.49941	0.50000	0.50058	0.50000	0.00566	0.00032
$23\pi/24$	0.00421	0.00428	0.99579	0.99572	0.00001	0.00089
$25\pi/24$	0.00420	0.00428	0.99580	0.99572	0.00010	0.00073

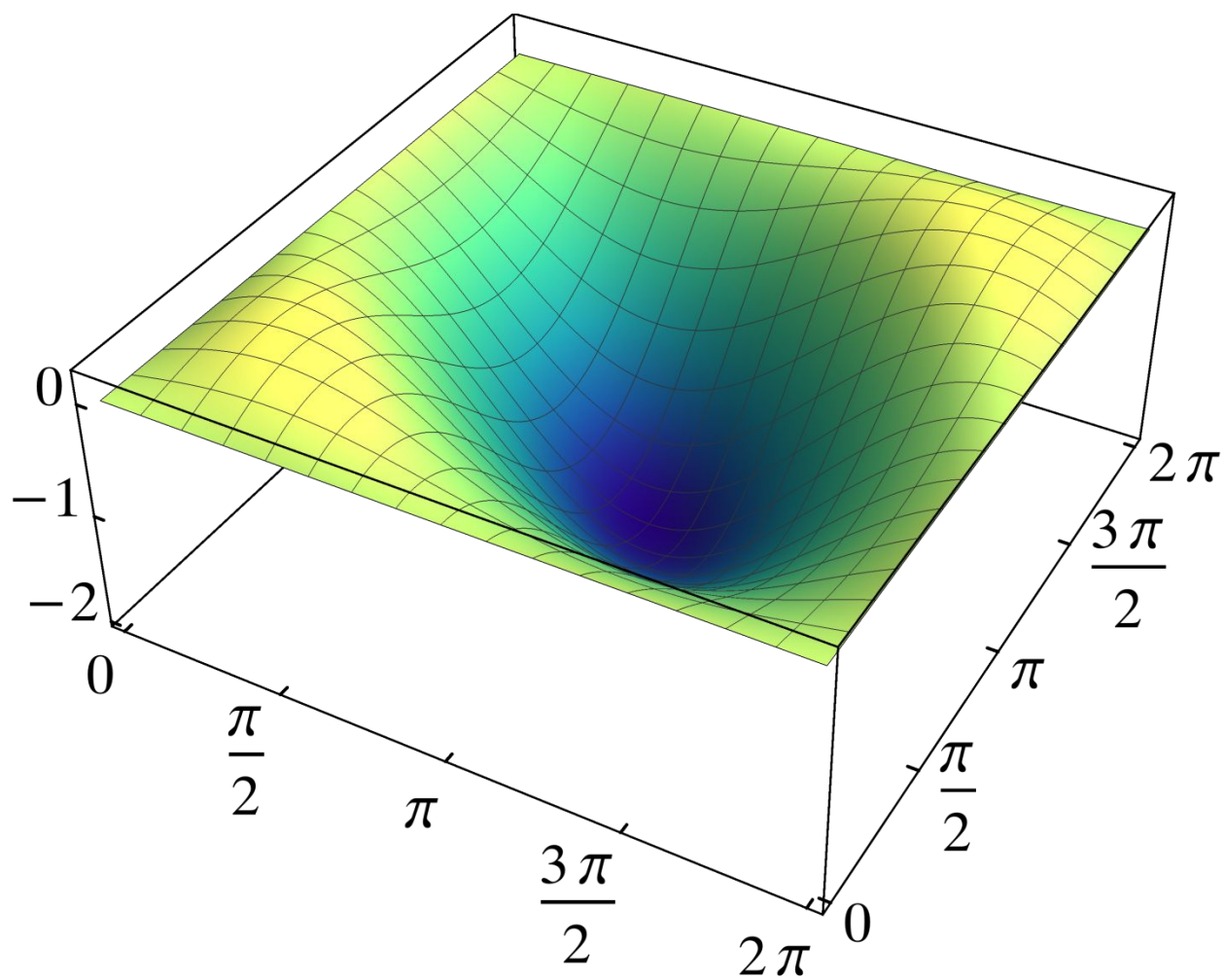
**Table 4.** Values of  $S = \langle \sigma_A \sigma_B \rangle + \langle \sigma_A \sigma_C \rangle + \langle \sigma_B \sigma_C \rangle - \langle \sigma_B \sigma_C \rangle$  in the CHSH inequality and the standard deviations  $\sigma$ . Values exceeding 2 show that a local hidden-variable theory cannot be formulated. Averages of 1000 combinations of runs on london.<sup>134</sup> Initial angle choices have been replaced by calculated angles that are predicted quantum mechanically to give identical correlations, as indicated. Asterisks denote values after error mitigation.

B, C angle	A, C angle	S	$\sigma(S)$	S*	$\sigma(S^*)$
$\pi$	$4\pi/3 \rightarrow 2\pi/3$	1.79995	0.02027	1.98703	0.02239
$25\pi/24 \rightarrow 23\pi/24$	$11\pi/8 \rightarrow 5\pi/8$	1.89699	0.02124	2.09490	0.02351
$13\pi/12 \rightarrow 11\pi/12$	$17\pi/12 \rightarrow 7\pi/12$	1.92583	0.02026	2.15255	0.02267
$9\pi/8 \rightarrow 7\pi/8$	$35\pi/24 \rightarrow 13\pi/24$	2.01277	0.02227	2.25173	0.02596
$7\pi/6 \rightarrow 5\pi/6$	$3\pi/2 \rightarrow \pi/2$	2.07908	0.02060	2.32884	0.02324
$29\pi/24 \rightarrow 19\pi/24$	$37\pi/24 \rightarrow 11\pi/24$	2.13133	0.02333	2.35556	0.02589
$5\pi/4 \rightarrow 3\pi/4$	$19\pi/12 \rightarrow 5\pi/12$	2.16123	0.02428	2.42166	0.02753
$31\pi/24 \rightarrow 17\pi/24$	$13\pi/8 \rightarrow 3\pi/8$	2.18799	0.02113	2.45229	0.02360
$4\pi/3 \rightarrow 2\pi/3$	$5\pi/3 \rightarrow \pi/3$	2.19123	0.03049	2.45518	0.03532
$11\pi/8 \rightarrow 5\pi/8$	$41\pi/24 \rightarrow 7\pi/24$	2.18970	0.02267	2.45280	0.02559
$17\pi/12 \rightarrow 7\pi/12$	$7\pi/4 \rightarrow \pi/4$	2.16072	0.02101	2.41939	0.02344
$35\pi/24 \rightarrow 13\pi/24$	$43\pi/24 \rightarrow 5\pi/24$	2.15274	0.02254	2.41180	0.02567
$3\pi/2 \rightarrow \pi/2$	$11\pi/6 \rightarrow \pi/6$	2.09914	0.02058	2.34854	0.02316
$37\pi/24 \rightarrow 11\pi/24$	$15\pi/8 \rightarrow \pi/8$	2.04815	0.02111	2.29119	0.02370
$19\pi/12 \rightarrow 5\pi/12$	$23\pi/12 \rightarrow \pi/12$	$\pi/3$	$\pi/12$	$\pi/3$	$5\pi/12$
$13\pi/8 \rightarrow 3\pi/8$	$47\pi/24 \rightarrow \pi/24$	$\pi/3$	$\pi/24$	$\pi/3$	$3\pi/8$
$5\pi/3 \rightarrow \pi/3$	$2\pi \rightarrow 0$	$\pi/3$	0	$\pi/3$	$\pi/3$
$41\pi/24 \rightarrow 7\pi/24$	$25\pi/24 \rightarrow 23\pi/24$	$\pi/3$	$23\pi/24$	$\pi/3$	$7\pi/24$
$7\pi/4 \rightarrow \pi/4$	$13\pi/12 \rightarrow 11\pi/12$	$\pi/3$	$11\pi/12$	$\pi/3$	$\pi/4$
$43\pi/24 \rightarrow 5\pi/24$	$9\pi/8 \rightarrow 7\pi/8$	$\pi/3$	$7\pi/8$	$\pi/3$	$5\pi/24$
$11\pi/6 \rightarrow \pi/6$	$7\pi/6 \rightarrow 5\pi/6$	$\pi/3$	$5\pi/6$	$\pi/3$	$\pi/6$
$15\pi/8 \rightarrow \pi/8$	$29\pi/24 \rightarrow 19\pi/24$	$\pi/3$	$19\pi/24$	$\pi/3$	$\pi/8$
$23\pi/12 \rightarrow \pi/12$	$5\pi/4 \rightarrow 3\pi/4$	$\pi/3$	$3\pi/4$	$\pi/3$	$\pi/12$
$47\pi/24 \rightarrow \pi/24$	$31\pi/24 \rightarrow 17\pi/24$	$\pi/3$	$17\pi/24$	$\pi/3$	$\pi/24$
$2\pi \rightarrow 0$	$4\pi/3 \rightarrow 2\pi/3$	$\pi/3$	$2\pi/3$	$\pi/3$	0

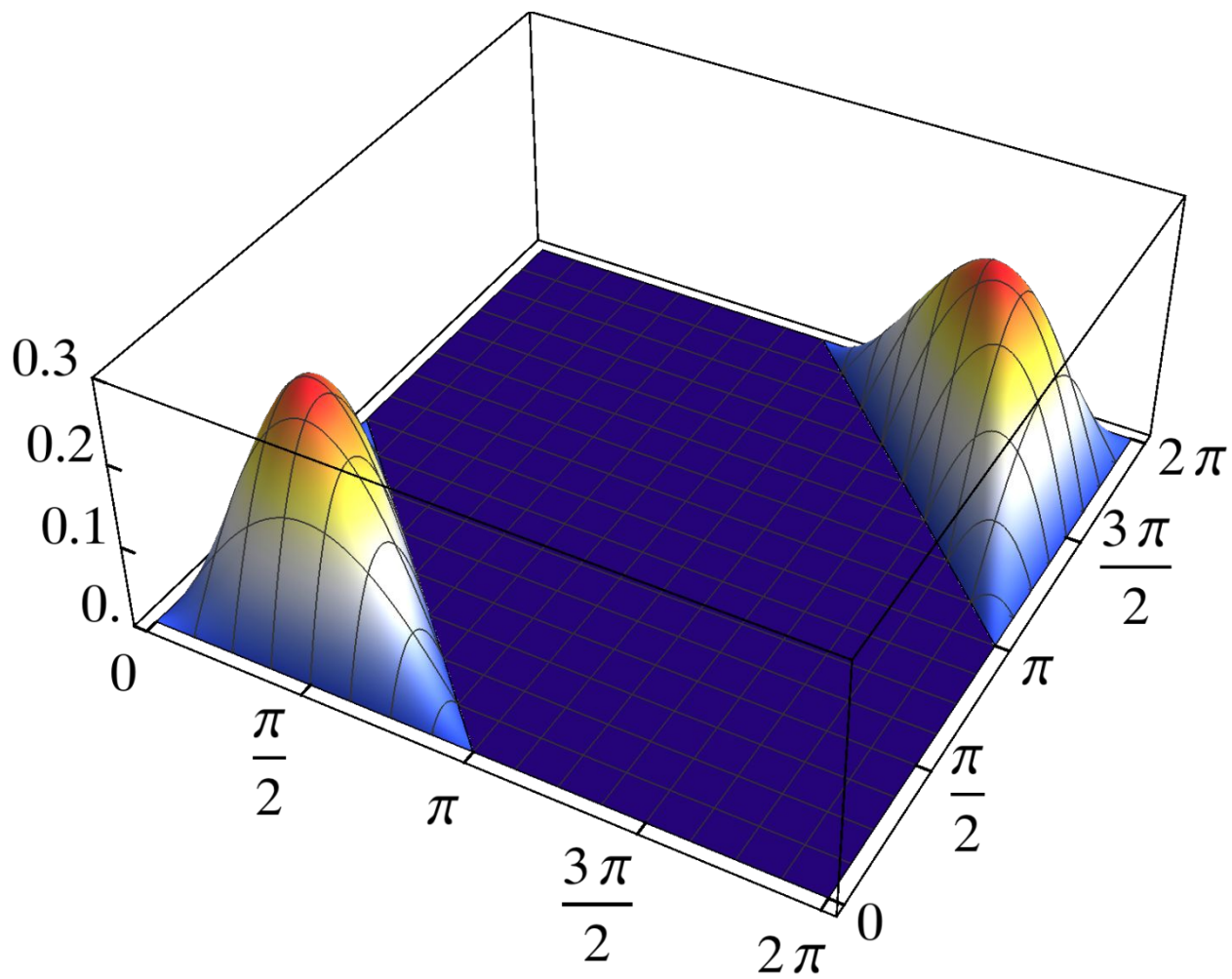


**Figure 1.** Histogram of the measurement outcomes  $|00\rangle$ ,  $|01\rangle$ ,  $|10\rangle$ , and  $|11\rangle$  for Bell states constructed with different methods (see text). Averaged results are shown for ten runs with 8192 shots each on the IBM quantum computing systems burlington,<sup>131</sup> vigo,<sup>132</sup> essex,<sup>133</sup> london,<sup>134</sup> and ourense.<sup>135</sup> Figure created with the IBM Q Experience.<sup>®</sup>

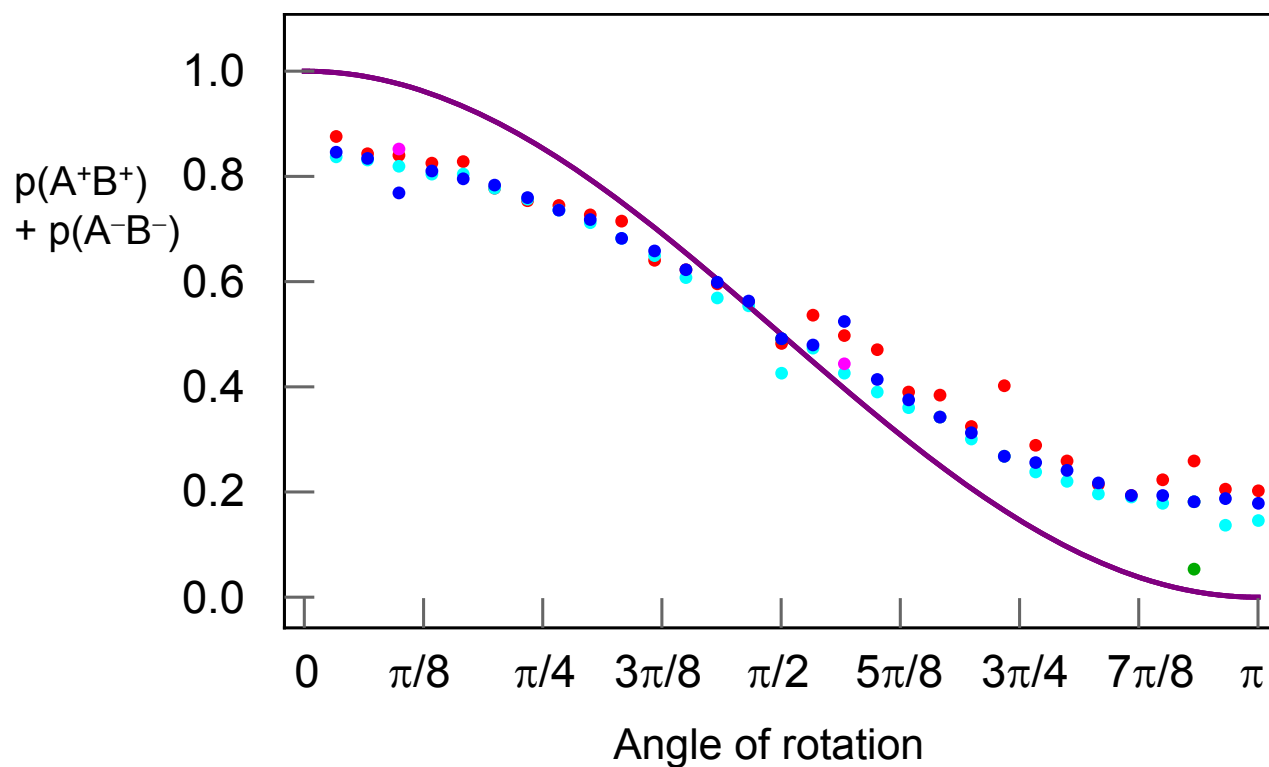




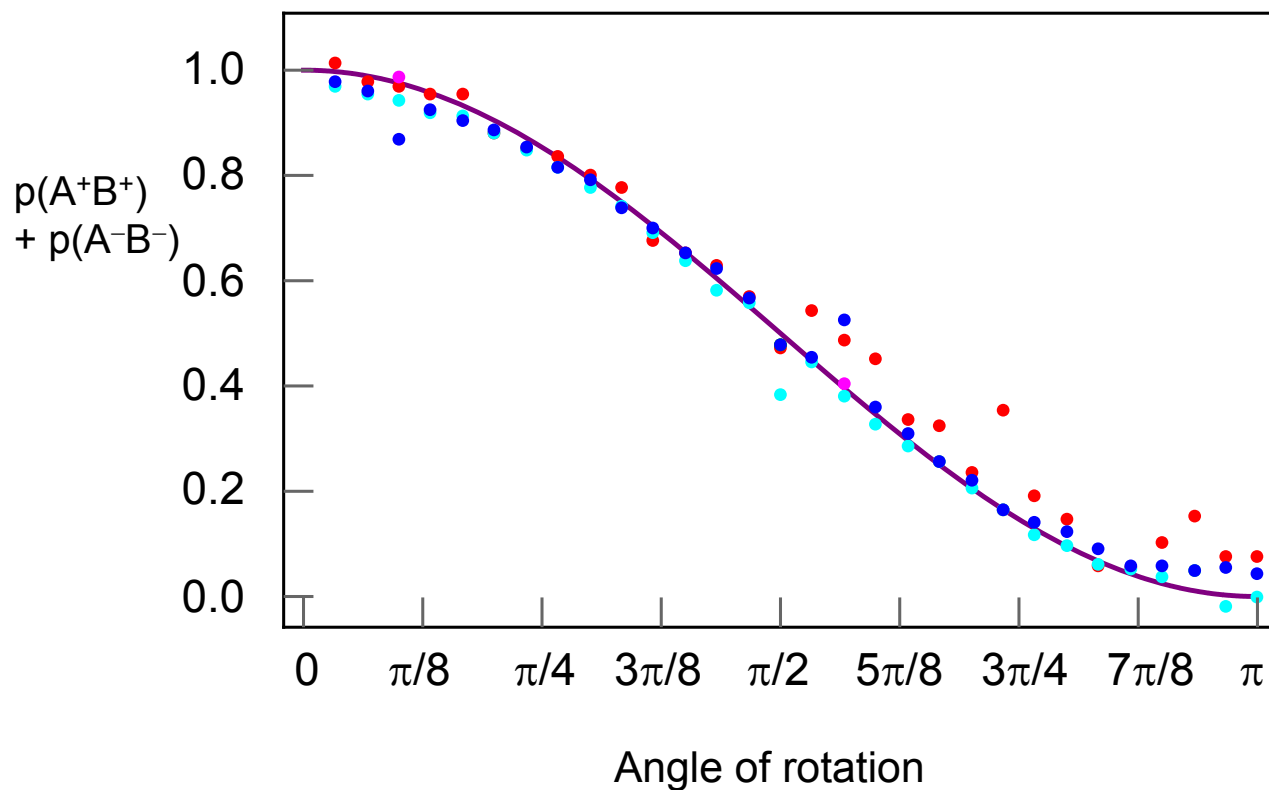
**Figure 2a.** Plot of the function  $f(\theta, \theta') \equiv \cos^2(\theta/2) - \cos^2[(\theta + \theta')/2] - \sin^2(\theta'/2)$ , as  $\theta$  and  $\theta'$  range from 0 to  $2\pi$ .



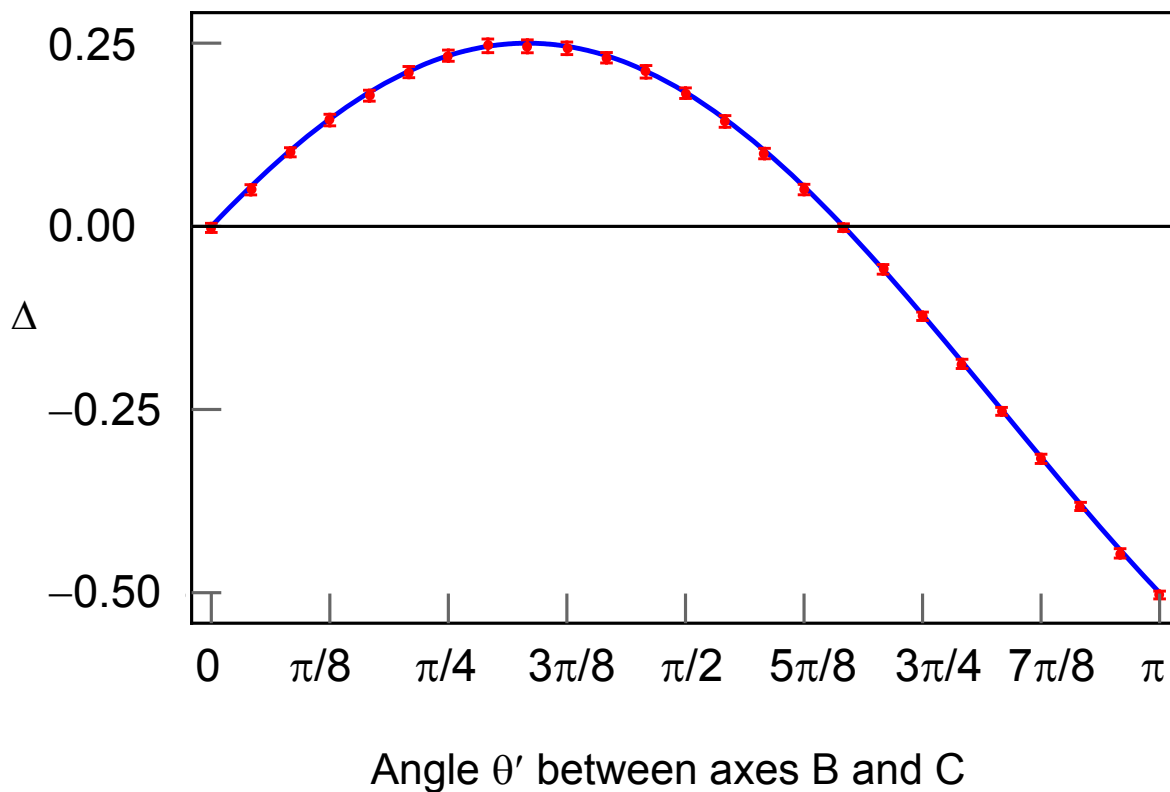
**Figure 2b.** Plot highlighting the regions where  $f(\theta, \theta') > 0$ , and the probabilistic inequality in Eq. (10) is violated. A cut-off is imposed in the horizontal plane, for all pairs of angles where  $f(\theta, \theta') < 0$ .



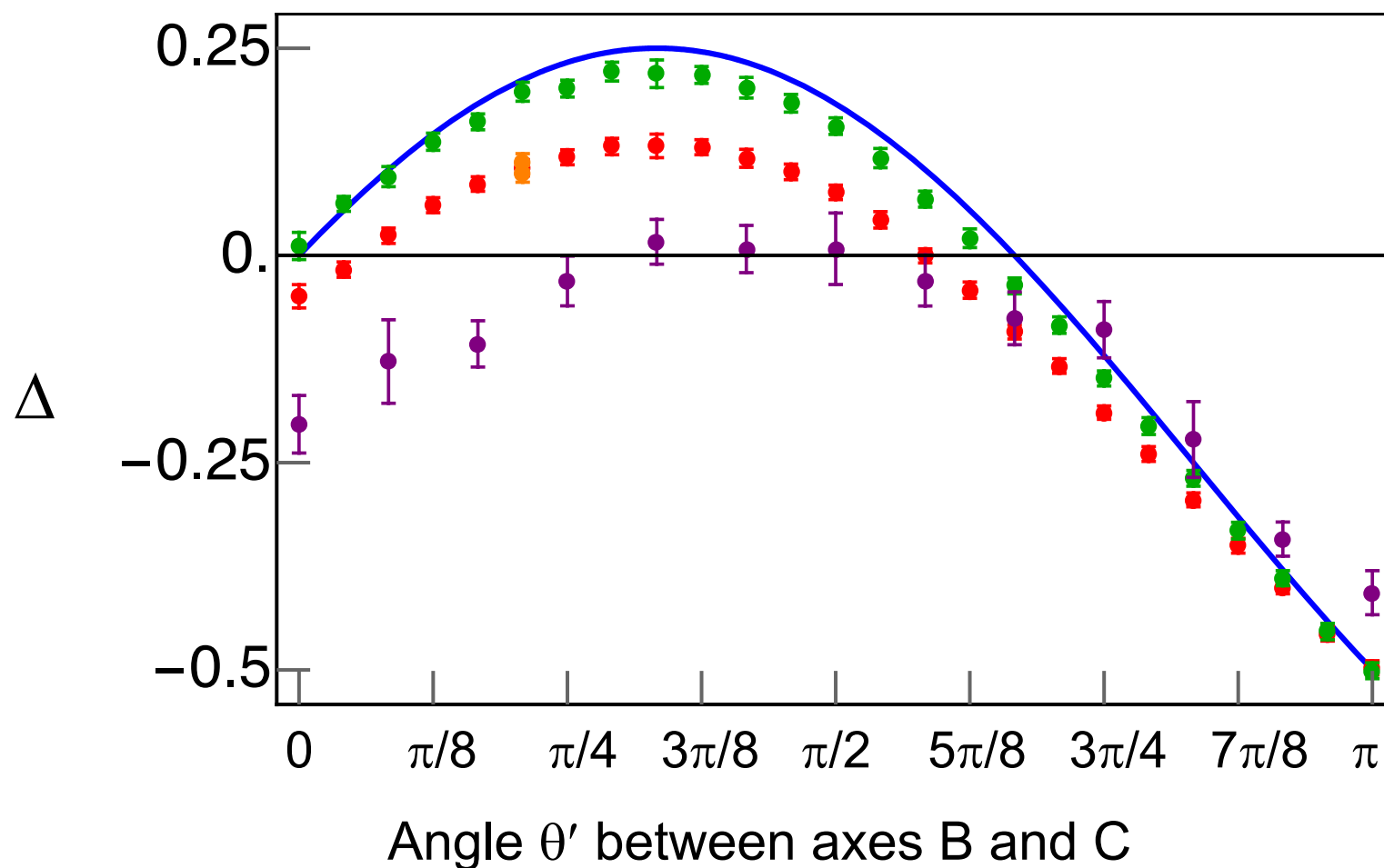
**Figure 3.** Values of  $p(A+B^+) + p(A-B^-)$  for the Bell states plotted as a function of the angle  $\theta$  between axes A and B, from sets of ten runs each on the burlington quantum computer<sup>131</sup> with 1024 shots (in red), 4096 shots (in cyan), and 8192 shots (in blue). Where outliers were observed in the initial runs, the outcomes of repeat runs are shown in green or magenta (see text for details). Purple curve: quantum mechanical predictions.



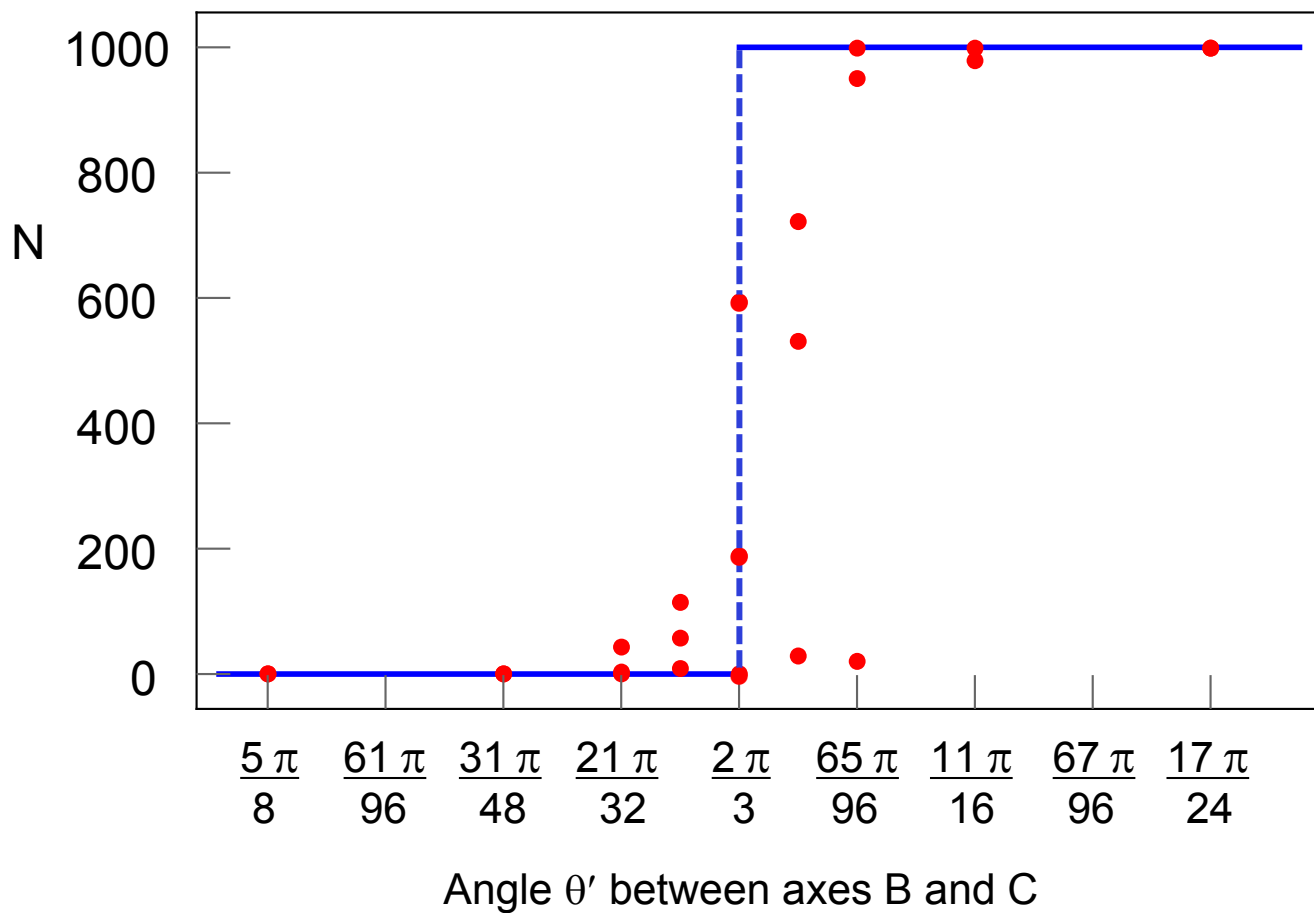
**Figure 4.** Error-mitigated values of  $p(A+B^+) + p(A-B^-)$  for the Bell states plotted as a function of the angle  $\theta$  between axes A and B, from sets of ten runs each on the burlington quantum computer<sup>131</sup> with 1024 shots (in red), 4096 shots (in cyan), and 8192 shots (in blue). As in Figure 3, where outliers were observed in the initial runs, the outcomes of repeat runs are shown in green or magenta (see text). Purple curve: quantum mechanical predictions.



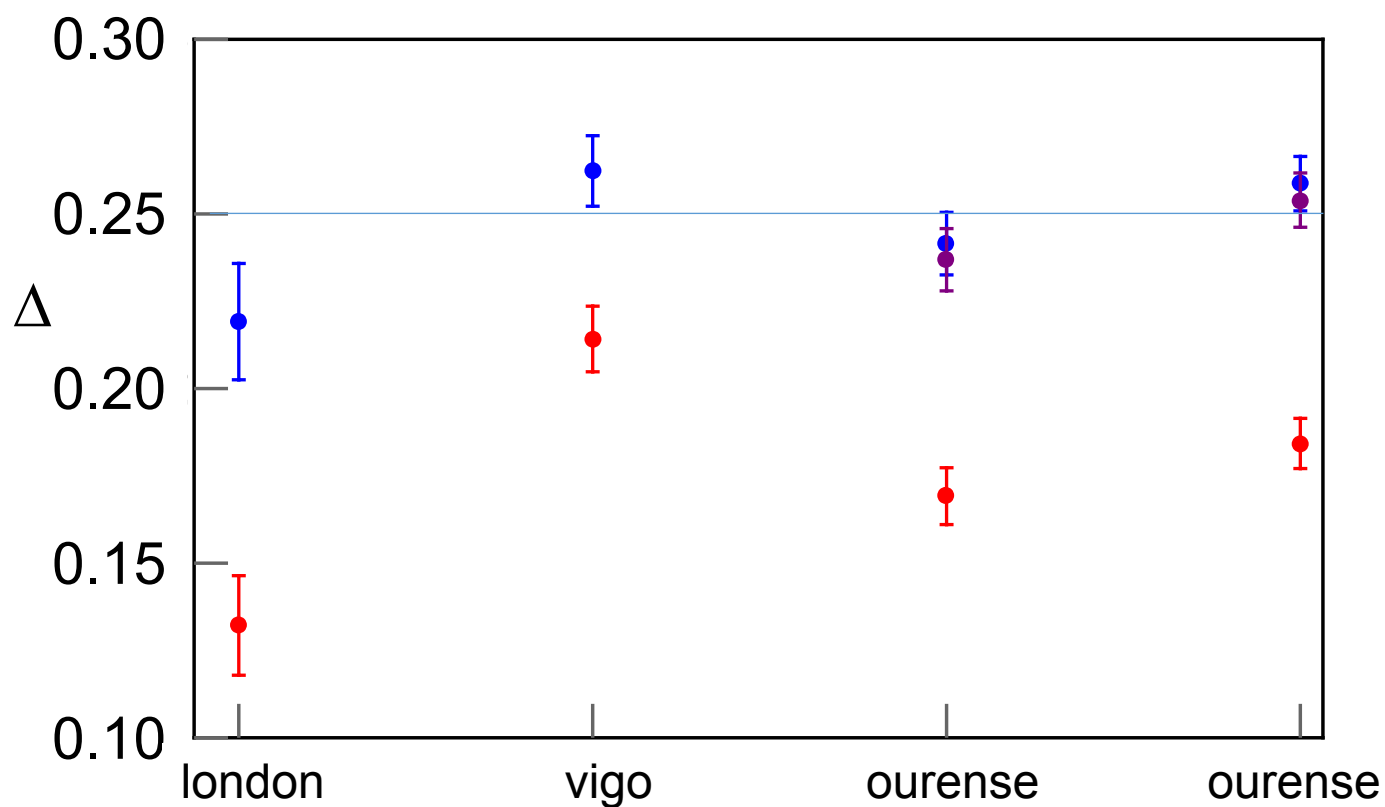
**Figure 5.** Average values of  $\Delta$  defined as  $\cos^2(\theta/2) - \cos^2[(\theta + \theta')/2] - \sin^2(\theta'/2)$  for the Bell states, as obtained from runs on the IBM qasm simulator.<sup>137</sup> The angle  $\theta$  between axes A and B is fixed at  $\pi/3$ , and the points are plotted in red as a function of the angle  $\theta'$  between axes B and C. Results from 1000 combinations of 10 runs each at angles  $\theta$ ,  $\theta'$  and  $(\theta + \theta')$ . The error bars reach one standard deviation above and below the average  $\Delta$  values. Blue curve: quantum mechanical predictions.



**Figure 6.** Average values of  $\Delta$  defined as  $\cos^2(\theta/2) - \cos^2[(\theta + \theta')/2] - \sin^2(\theta'/2)$  for the Bell states, as obtained from runs on the IBM london<sup>134</sup> quantum computer. Results from 1000 combinations of 10 runs each at angles  $\theta$ ,  $\theta'$  and  $(\theta + \theta')$ . The angle  $\theta$  between axes A and B is fixed at  $\pi/3$ , and the raw data points are plotted in red as a function of the angle  $\theta'$  between axes B and C. Error-mitigated points are plotted in green. See text for orange and magenta points. The error bars reach one standard deviation above and below the average  $\Delta$  values. Blue curve: quantum mechanical predictions.

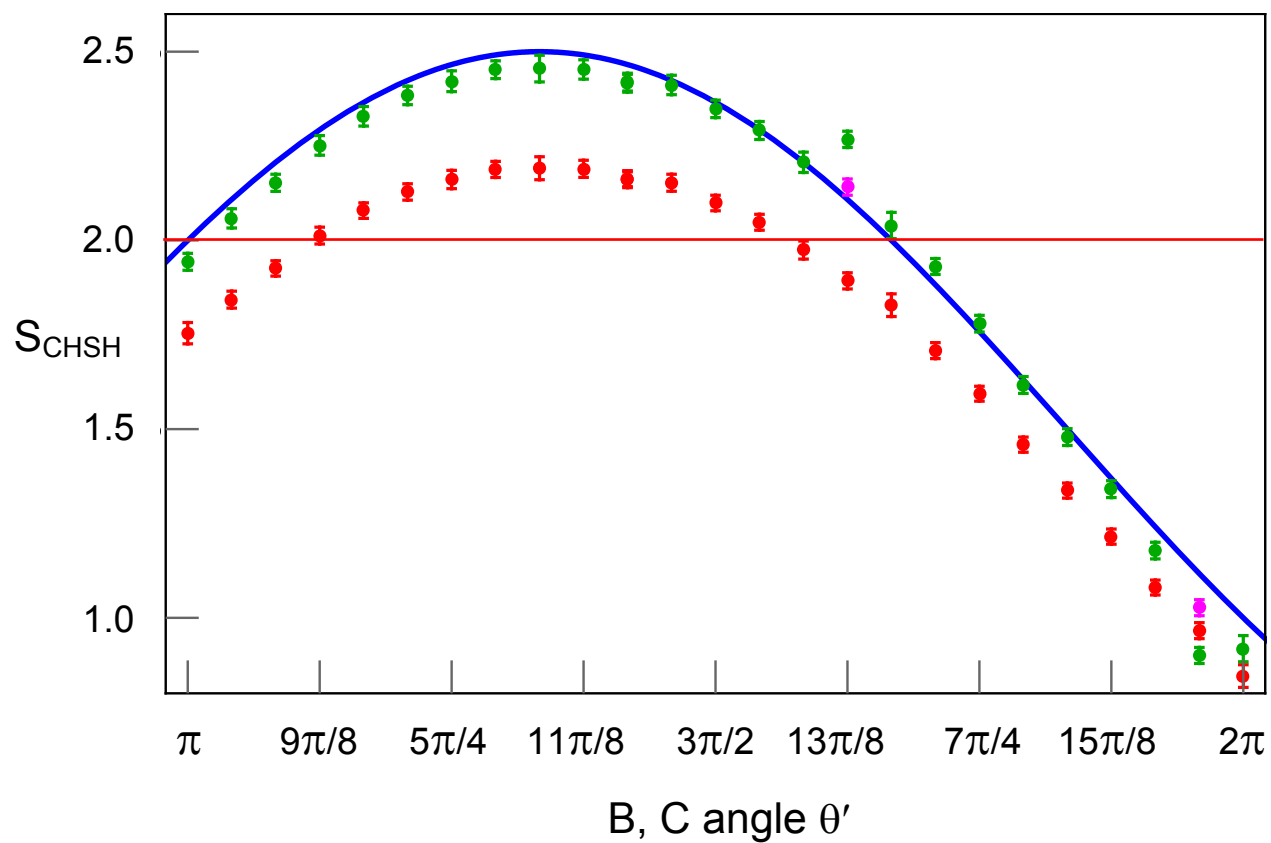


**Figure 7.** Number of cases where the quantum computer gave negative values of  $\Delta$ , out of 1000 cases generated by taking all possible combinations of 10 runs for each of the pairs of angles (A, B), (B, C), and (A, C). Results from multiple calculations are plotted as a function of the angle  $\theta'$  between axes B and C. Calculations run on the IBM ourense<sup>135</sup> quantum computer.



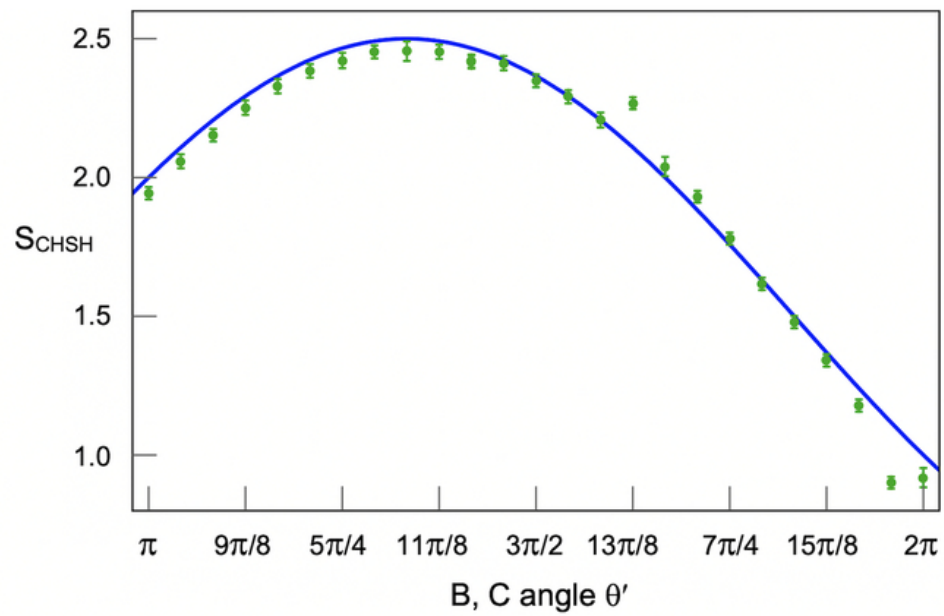
**Figure 8.** Calculated  $\Delta$  values for  $\theta' = \pi/3$ , obtained from runs on london,<sup>134</sup> vigo,<sup>132</sup> and ourense<sup>135</sup> with and without error mitigation (see text). The maximum value predicted quantum mechanically is  $\Delta = 0.25$ .





**Figure 9.** Raw results (red) and the error-mitigated results (green) for  $S$  in the CHSH inequality of Eq. (11), from runs on ourense,<sup>135</sup> plotted as a function of the angle  $\theta'$  between axes B and C. Values of  $S > 2$  rule out local hidden-variable theories. For the two results plotted in magenta, see text.

Results for the linear combination  $S$  of spin-projection correlation functions in the Clauser-Horne-Shimony-Holt inequality, from runs on a publicly accessible IBM quantum computer after error mitigation. Values of  $S > 2$  rule out local hidden-variable theories.



57x39mm (300 x 300 DPI)